

TOPICAL REVIEW

## Review of lead-free Bi-based dielectric ceramics for energy-storage applications

To cite this article: Lisong Li *et al* 2021 *J. Phys. D: Appl. Phys.* **54** 293001

View the [article online](#) for updates and enhancements.







**IOP | ebooks™**

Bringing together innovative digital publishing with leading authors from the global scientific community.

Start exploring the collection—download the first chapter of every title for free.

## Topical Review

# Review of lead-free Bi-based dielectric ceramics for energy-storage applications

Lisong Li<sup>1,2</sup>, Pengyuan Fan<sup>1,2,\*</sup>, Mengqi Wang<sup>1,2</sup>, Naohisa Takesue<sup>3</sup> , David Salamon<sup>4</sup>, Alexander N Vtyurin<sup>5</sup>, Yangjun Zhang<sup>6,\*</sup>, Hua Tan<sup>1,2</sup>, Bo Nan<sup>1,2</sup> , Ya Lu<sup>2</sup>, Laijun Liu<sup>7</sup>  and Haibo Zhang<sup>1,2,\*</sup> 

<sup>1</sup> School of Materials Science and Engineering, State Key Laboratory of Material Processing and Die and Mould Technology, Huazhong University of Science and Technology, Wuhan 430074, People's Republic of China

<sup>2</sup> Guangdong HUST Industrial Technology Research Institute, Dongguan 523808, People's Republic of China

<sup>3</sup> Faculty of Science, Fukuoka University, Fukuoka 814-0180, Japan

<sup>4</sup> Central European Institute of Technology (CEITEC) Brno University of Technology, Brno, Czech Republic

<sup>5</sup> Kirensky Institute of Physics SB RAS, Akademgorodok 50/38, Krasnoyarsk 660036, Russia

<sup>6</sup> State Key Laboratory of Automotive Safety and Energy, School of Vehicle and Mobility, Tsinghua University, Beijing 100084, People's Republic of China

<sup>7</sup> Guangxi Key Laboratory of Optical and Electronic Materials and Devices, Guilin University of Technology, Guilin 541004, People's Republic of China

E-mail: [pyfan@hust.edu.cn](mailto:pyfan@hust.edu.cn), [yjzhang@tsinghua.edu.cn](mailto:yjzhang@tsinghua.edu.cn) and [hbzhang@hust.edu.cn](mailto:hbzhang@hust.edu.cn)

Received 8 November 2020, revised 16 March 2021

Accepted for publication 15 April 2021

Published 13 May 2021



CrossMark

## Abstract

Dielectric energy-storage ceramics have the advantages of high power density and fast charge and discharge rates, and are considered to be excellent candidate materials for pulsed power-storage capacitors. At present, the application of dielectric energy-storage ceramics is hindered by their low energy density and the fact that most of them contain elemental lead. Therefore, lead-free dielectric energy-storage ceramics with high energy storage density have become a research hot spot. In this paper, we first present the requirements that dielectric energy-storage capacitors impose on the properties of ceramic materials. We then review our previous research work combined with research progress into bismuth (Bi)-based lead-free energy-storage ceramics including  $\text{Bi}_{0.5}\text{Na}_{0.5}\text{TiO}_3$  (BNT),  $\text{BiFeO}_3$ , and  $\text{Bi}_{0.2}\text{Sr}_{0.7}\text{TiO}_3$ , in which the composition design ideas and related energy-storage characteristics of BNT-based lead-free energy-storage ceramics are emphasized. At the same time, we highlight the problems faced by Bi-based lead-free energy-storage ceramics and some strategies for addressing them. Finally, we examine the future prospects of research into Bi-based lead-free energy-storage ceramics.

Keywords: dielectric materials, energy storage, lead-free, Bi-based ceramics

(Some figures may appear in colour only in the online journal)

\* Authors to whom any correspondence should be addressed.

## 1. Introduction

Electric energy storage is an important topic in the field of energy storage, along with fossil energy, solar energy, and wind energy [1, 2]. Electric energy storage includes dielectric capacitors, electrochemical capacitors, chemical cells, solid-oxide fuel cells, flywheels, superconducting energy-storage systems, etc. Among these, dielectric capacitors have attracted more and more attention due to their high power density ( $\sim 10^8$  MW kg $^{-1}$ ), fast charge and discharge times ( $< 1$   $\mu$ s), and excellent cycle times ( $\sim 10^5$ ) [3–6]. At the same time, they are considered to have great application prospects in fields such as pulsed power supplies, power devices, lasers, accelerators, etc. However, at the moment, the effective energy density of dielectric capacitors ( $W_{\text{rec}}$ ) is relatively low ( $10^1 \sim 10^2$  Wh kg $^{-1}$ ) [7, 8], and they cannot satisfy the demands of integrated, lightweight, and miniaturized pulse power devices. Hence, research into improving the effective energy density  $W_{\text{rec}}$  has been considered to be a hot topic in the field of functional materials [9–11].

Common capacitor materials in use include glass, polymers, ceramics, ceramic–polymer composites, and glass–ceramic composites. Polymers and glass matrices generally possess a high breakdown strength but a low permittivity [12]; ceramics have a high permittivity but a low breakdown strength. Organic polymers, such as poly vinylidene fluoride, polypropylene, and polybutadiene, etc, have a high breakdown strength, usually close to 6000 kV cm $^{-1}$ , due to their particular structure [13]. However, the dielectric permittivity of polymers is not high, their thermal stability is poor, and they decompose easily when the temperature is slightly high. Glass is also a high-performance energy-storage material, but its high performance can only be realized under extremely high electric fields, and it can easily cause electrical fatigue and destructive and irreversible electrical breakdown. These cause problems for both production and use. Ceramics have excellent thermal stability properties, the best heat resistance, and, moreover, can be used over a wide temperature range [14–18]. In addition, dielectric ceramics have a medium breakdown strength ( $E_b$ ), low dielectric loss, good fatigue resistance, and they can better meet the requirements of energy-storage capacitors in aerospace, oil drilling, electromagnetic pulse weapons and other fields [19]. Hence, dielectric ceramics are considered to be an optimal material for preparing high-temperature dielectric pulsed-power energy-storage capacitors.

In addition, based on the thickness of dielectric ceramics, they can be divided into thin-film ceramics (with a thickness of less than 1  $\mu$ m), thick-film ceramics (with thicknesses between 1  $\mu$ m and 100  $\mu$ m) and bulk ceramics (with thickness larger than 100  $\mu$ m). Due to their reduced porosity and defects, thin-film ceramics have large  $E_b$  and  $W_{\text{rec}}$ . However, as they are restricted by their thickness, the energy storage of thin-film ceramics is low, and their preparation process is complex. Hence, it is difficult to prepare large-scale samples. In addition, thin-film ceramics call for difficult preparation conditions. As a result, their application is restricted

to some specialized fields, such as medical shock apparatus, etc. The thickness of thick-film ceramics is in between those of thin-film ceramics and bulk ceramics, and thick-film ceramics possess the advantages of both. Compared to bulk ceramics, thick-film ceramics possess high  $E_b$  and small scale, and are convenient for the integration and miniaturization of equipment. In addition, thick-film ceramics can be made into multilayer structures, which possess greater thickness and energy-storage density. By comparison, the preparation of bulk ceramics is simple and low cost, their mechanical strength is high, their temperature stability is good, and their total energy-storage density is excellent. If bulk ceramics made from directed materials possessed excellent energy-storage properties, then thin-film and/or thick-film ceramics made of the same material would have higher  $W_{\text{rec}}$ . In other words, to study the properties of bulk ceramics, it is beneficial for us to thoroughly research thin-film and thick-film ceramics.

Due to their great advantages in terms of cycle times, lifetimes, and thermal stability, dielectric ceramics have been extensively studied in recent years. Among them, PbTiO $_3$ , PbZrO $_3$  and other Pb-based energy-storage materials have been widely used in production due to their high polarizability, large dielectric permittivity (the highest is up to 2100), excellent cycle life, and charge–discharge time [20]. However, they are harmful to the environment and the human body. Furthermore, with the promulgation of bans, lead-free electronic ceramics have become an unavoidable trend. In addition, the mass density of lead-free materials is usually lower than 5.5 g cm $^{-3}$ . Compared with the mass density (7.5 g cm $^{-3}$ ) of Pb-based ceramics, for the same  $W_{\text{rec}}$ , lead-free ceramics can better satisfy the demand for lightweight pulse power equipment. Hence, the search for lead-free bulk ceramics with high energy-storage density is of great importance.

In terms of lead-free ceramics, many studies have been performed, as shown in figure 1. It has recently been reported that energy storage using lead-free anti-ferroelectric (AFE) AgNbO $_3$  (AN)-based ceramics has achieved 7.01 J cm $^{-3}$  for an applied field of 476 kV cm $^{-1}$  [21], which is comparable to Pb-based materials in terms of energy density. However, under small electric fields, the energy storage properties of Pb-based materials possess unique advantages as shown in figure 1. Lead-free energy-storage materials are far from being able to meet practical needs. In addition, other than AN-based and NaNbO $_3$  (NN)-based AFE materials, bismuth (Bi)-based ceramics, such as Na $_{0.5}$ Bi $_{0.5}$ TiO $_3$ , BiFeO $_3$  (BF), Bi $_{0.2}$ Sr $_{0.7}$ TiO $_3$ , etc, have not attracted enough attention and have not been extensively studied. Na $_{0.5}$ Bi $_{0.5}$ TiO $_3$ , BF, etc, have usually been considered to have a high energy-storage performance due to their strong polarization (for example, 100  $\mu$ C cm $^{-2}$ ) corresponding to a large  $P_{\text{max}}$ . Besides, over the last year, the main trend of the lead-free energy-storage field has been to focus on polymer or ceramic–polymer composites. There has been little focus on Bi-based energy-storage ceramics. With the rapid development of lead-free dielectric ceramics, more Bi-based dielectric ceramics have come to possess excellent properties. Combining the research of our group, we provide an overview of the current development of Bi-based

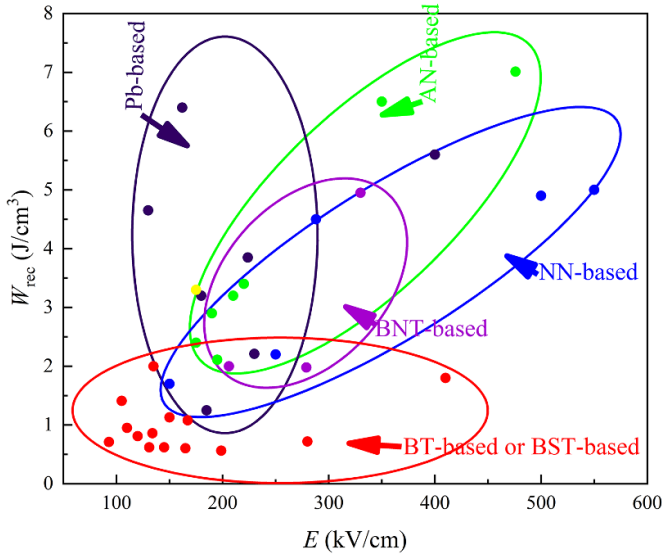


**Figure 1.** Lead-free ceramic energy storage performance [17, 20–56].

ceramics, and highlight their challenges, strategies, and future development. Hopefully, this will provide a reference for those seeking high-energy-storage lead-free dielectric materials.

## 2. Basic principles of dielectric energy storage

### 2.1. The principles of dielectric energy storage

The energy-storage performance of dielectric capacitors is directly related to their dielectric constant and breakdown strength [13]. For nonlinear dielectric materials, the polarization  $P$  increases to a maximum polarization  $P_{\max}$  during charging. Different materials have different  $P_{\max}$ , and a large  $P_{\max}$  is necessary for high-density energy storage. During discharge, the polarization decreases to a non-zero remanent polarization  $P_r$ . Hence, the energy stored in the capacitor cannot be completely released [56]. For nonlinear dielectrics, the total energy-storage density due to charging is denoted by  $W_{\text{total}}$ , and the energy storage that can be released during discharge is called the effective energy density,  $W_{\text{rec}}$ . The energy storage that cannot be released is denoted by  $W_{\text{loss}}$ . The ratio of  $W_{\text{rec}}$  and  $W_{\text{total}}$  is called the energy-storage efficiency,  $\eta$ . By definition,  $W_{\text{total}}$ ,  $W_{\text{rec}}$  and  $\eta$  are related as follows [56]:

$$W_{\text{total}} = \int_0^{P_{\max}} E dp \quad (1)$$

$$W_{\text{rec}} = \int_{P_r}^{P_{\max}} E dp \quad (2)$$

$$\eta = W_{\text{rec}}/W_{\text{total}} \quad (3)$$

where  $P$  is the polarization,  $P_{\max}$  is the maximum polarization and  $P_r$  is the remanent polarization. The effective energy density is determined by the breakdown strength

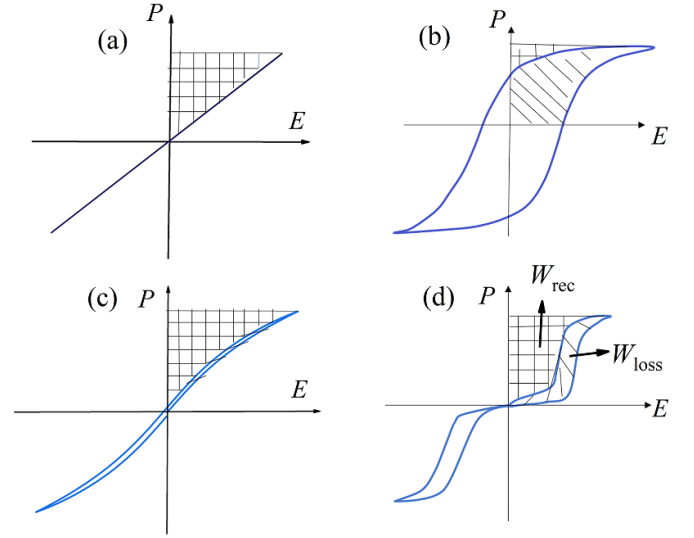


**Figure 2.** Hysteresis loops of (a) a linear dielectric (b) ferroelectrics (FEs) (c) a relaxor FEs (RFEs) (d) AFE.

(abbreviated as  $E_{\text{BDS}}$ ) and  $\Delta P$ , where  $\Delta P$  is equal to  $P_{\max} - P_r$ .

### 2.2. Types of dielectric energy storage

The energy-storage density of a dielectric material can be obtained by calculating the area enclosed by  $P$ - $E$  in the hysteresis loop. As shown in figure 2, the mesh shadow area formed by the upper half of the hysteresis loop and the  $P$  axis represents the effective energy-storage density ( $W_{\text{rec}}$ ). The obliquely shaded area enclosed by the hysteresis loop itself is the loss energy density ( $W_{\text{loss}}$ ) caused by thermal effects and dielectric loss during charging and discharging. In brief, the energy-storage density and efficiency are jointly determined by the maximum polarization ( $P_{\max}$ ), the remanent polarization ( $P_r$ ) and the breakdown strength ( $E_b$ ).

Dielectric energy-storage materials can be divided into four types [13, 19, 56]: linear dielectrics, ferroelectrics (FEs), relaxor FEs (RFEs) and AFEs. (a) The dielectric constant of linear dielectrics is independent of their electric field, and the polarization is linearly related to the applied electric field strength. The energy density can be simplified to  $J = \frac{1}{2} \epsilon_0 \epsilon_r E^2$ . As shown in figure 2(a), linear dielectrics, such as  $\text{CaTiO}_3$  (CT) and  $\text{SrTiO}_3$  (ST), etc, [13] possess high breakdown strength  $E_b$ , low polarization, low loss, and high energy-storage efficiency [57, 58]. For them, the key to increasing the energy-storage property is to increase  $P_{\max}$ ; (b) FEs are materials in which the direction of spontaneous polarization can be reversed by an applied electric field [19]. As shown in figure 2(b), FEs have relatively high polarization. However, due to their large long-range domains, which are difficult to rotate, the remanent polarization is also large when the electric field is removed. Therefore, the energy-storage density and efficiency of FEs are not desirable; (c) RFEs are materials with diffusive FE phase transitions. They exhibit a broader

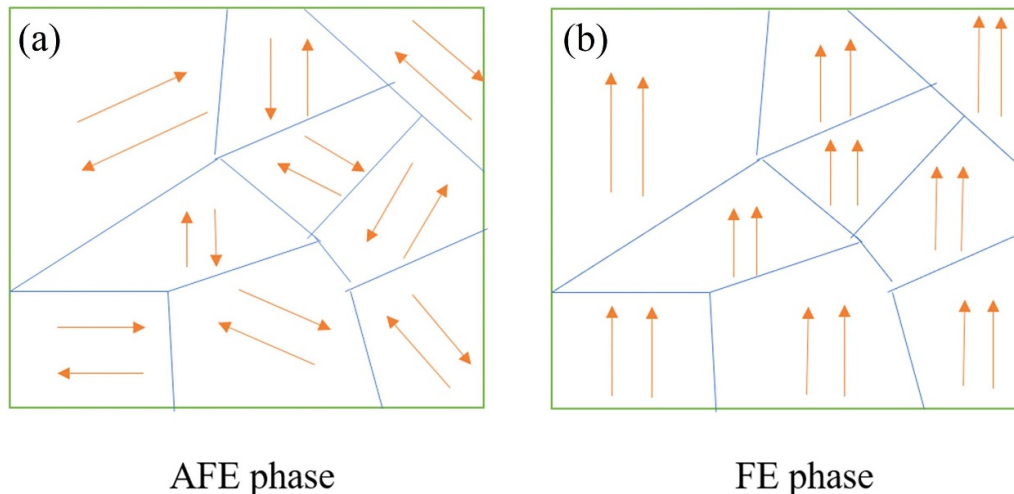


**Figure 3.** Variations of AFE domains with an applied electric field.

dielectric peak and a greater frequency dispersion [19]. The hysteresis loop of an RFE is shown in figure 2(c). Unlike the large long-range domains of FEs, structural disorder and highly dynamic polar nanoregions (PNRs) have been observed in RFEs [19]. In an RFE, when the electric field is applied, the PNRs combine in the same orientation. Once the electric field is removed, the PNRs of RFEs can quickly return to their original disordered state, resulting in a smaller remanent polarization and a slimmer hysteresis loop. Therefore, RFEs have better energy-storage properties than FEs and are considered to be one of the most promising dielectric energy-storage materials; (d) AFE is a kind of dielectric material with antiparallel dipoles and zero spontaneous polarization [56]. It has a large  $P_{\max}$ , a small  $P_r$ , and notable double polarization–electric field ( $P$ – $E$ ) loops, as shown in figure 2(d). When an electric field is applied, its behavior is similar to a linear dielectric to begin with, and the polarization  $P$  has a linear relationship with the electric field  $E$ . When the electric field is higher than a critical value, characteristics similar to those of FEs appear. From a microscopic perspective, when the initial electric field is small (at the beginning), the adjacent lattices of AFEs are opposite to the electric dipole moments, and cancel each other out, as shown in figure 3(a). The AFE phase does not show spontaneous polarization at this time. When the applied electric field is higher than a certain critical value, as shown in figure 3(b), the FE phases tend to align in the same direction under the effects of the external electric field, and the AFE phase becomes an FE phase. At the same time, the polarization increases sharply. When the applied electric field is removed, the FE changes to an AFE, and a small remanent polarization is obtained. Therefore, AFEs such as  $\text{PbZrO}_3$ , AN, etc, have large energy-storage capacities. However, during the transition from an AFE to an FE, the loss is large, and the energy-storage efficiency is low. Hence, the reversible phase-transition lag leads to a poor fatigue performance.

### 2.3. Microstructure of ceramics

For ceramic energy storage, another important factor that determines the energy-storage density is the microstructure of ceramics. Examples include the crystal phase, glass phase, gas phase, domain walls, etc. The crystal phase is the main component phase and the carrier that realizes various functions, such as polarization. The glass phase is the part of a ceramic that is composed of an amorphous solid structure. The main function of the glass phase is to fill the gaps between the crystal phases and bond the dispersed crystal phases, thereby improving the density of the material, preventing crystal transformation, and restraining grain growth. Moreover, the glass phase can reduce the sintering temperature and promote sintering. The gas phase is a kind of gas in ceramic materials. It is the result of pores entering the grain or the interstices caused by the rapid movement of the grain boundary during grain growth. Pores in a grain boundary can be eliminated by grain boundary diffusion. In sintering, pores can prevent the grain from moving too fast and can pin the grain boundary so the grain can be refined to a certain extent. In addition, much effort in the search for lead-free dielectric ceramics with high energy-storage density has focussed on solid solutions that exhibit a morphotropic phase boundary (MPB). Some excellent performance often occurs in the MPB. Meanwhile, the domain walls make a large contribution to the dielectric and the breakdown strength.

## 3. Bi-based dielectric ceramics and energy storage properties

### 3.1. $\text{Bi}_{0.5}\text{Na}_{0.5}\text{TiO}_3$ -based ceramics

**3.1.1. Phase structure.**  $\text{Bi}_{0.5}\text{Na}_{0.5}\text{TiO}_3$  (BNT) is a perovskite FE with a substitution in the A-site ion complex; Bi and Na co-occupy the A-site. BNT was first synthesized in 1960



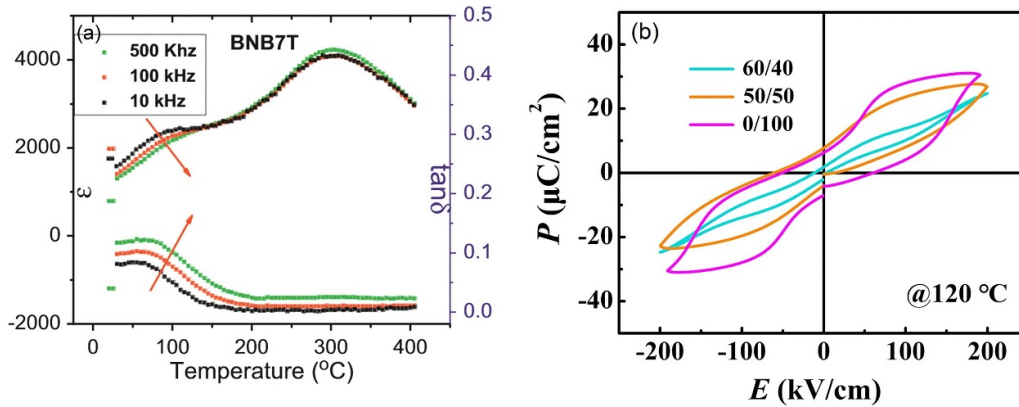


**Figure 4.** Dielectric temperature spectrums and polarization curves. (a) Dielectric temperature spectrum of 0.93 % BNT–0.07 % BT. Reprinted from [71], Copyright (2013), with permission from Elsevier. (b) Polarization curve of BNT–NN (BT—BaTiO<sub>3</sub>, NN—NaNbO<sub>3</sub>). Reproduced from [9] with permission of The Royal Society of Chemistry.

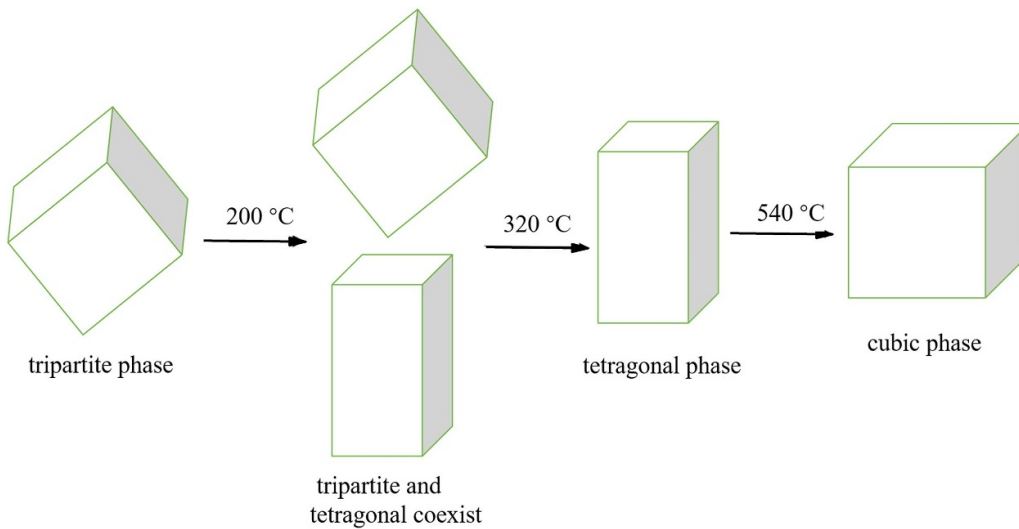


**Figure 5.** Phase transitions of BNT.

by Smolenskii *et al* [59]. At room temperature, BNT belongs to the rhombohedral system ( $a = 0.3886$  nm,  $\alpha = 89.16^\circ$ ), its  $P_r$  is about  $38 \mu\text{C cm}^{-2}$  [60, 61], the relative dielectric permittivity is about 240–340, and the Curie temperature is as high as  $320$  °C– $340$  °C [62, 63]. In 1962, Bührer [64] explained the FE origin of BNT, and believed that the ferroelectricity of BNT originated from the specific electronic structure, which is similar to that of  $\text{Pb}^{2+}$ , which also gave BNT a high polarizability [65, 66]. At the same time, similarly to  $\text{BaTiO}_3$  (BT), the displacement polarization of the  $\text{Ti}^{4+}$  ion in the central B-site produces ferroelectricity. The phase-transition process of BNT is complex, and the unique double hysteresis loop of its beam waist has attracted the attention of many researchers [67]. It is debatable whether BNT is tetragonal or rhombohedral at  $200$  °C– $320$  °C or whether it is in the relaxor state of coexistence in this wide temperature range.

In 1980, Zvirgzds *et al* [68] studied the phase transition of a BNT single crystal by x-ray diffraction. It was found that the BNT grains changed from a cubic FE structure to a tetragonal

FE structure near  $540$  °C and from a tetragonal to a rhombohedral phase structure near  $260$  °C. In 1986, Zhang *et al* [69] analyzed the phase transition of BNT single-crystal ceramics by Raman spectroscopy, and found that BNT changed from mainly cubic to tetragonal at  $564$  °C while it was mainly tetragonal to rhombohedral at  $311$  °C. Moreover, in the dielectric temperature spectrum of BNT, there are two obvious peaks of dielectric permittivity [70, 71],  $T_s$  and  $T_m$ , as shown in figure 4. This led some researchers to believe that, at  $200$  °C, the FE phase changed into an AFE phase.

In the temperature range of  $T_s \sim T_m$ , the  $P$ – $E$  curve is similar to the double hysteresis loop. The two dielectric peaks in the dielectric spectrum versus temperature are considered to be responses to the two-phase transitions in BNT, and the temperature range  $T_s \sim T_m$  is considered to be an AFE phase region [72]. However, in subsequent studies, a growing number of researchers believed that the transformation of BNT from its tetragonal phase to its rhombohedral phase was a slow process in the range between  $200$  °C and  $320$  °C. As shown in figure 5, the two structures coexist over a wide temperature

range in the form of PNRs [73–75], thus forming a two-peak dielectric spectrum with temperature and the hysteresis loop of the beam waist. There was no AFE phase in BNT, and BNT was simply an RFE [74, 76].

Following an XRD analysis in 1995, Suchanicz and Kwapulinski [74] believed that BNT was a cubic structure above 500 °C. Meanwhile, between 500 °C and 420 °C, it was a pure tetragonal structure. In the vicinity of 320 °C, the quadripartite and rhombohedral phases coexist, each accounting for one half of the volume. When the temperature drops to 280 °C, the tetragonal volume fraction of BNT decreases to 20%. Ma and Tan [77] found that with an increase in Ba in the BNT–BT system, its structure changed from the FE phase (R3c) to the tetragonal AFE phase (P4bm), which resulted in the existence of two MPBs in the BNT–BT system, R3c–P4bm and P4bm–P4mm. At the same time, the tetragonal AFE sequences were limited by the nanodomains, which resulted in dielectric relaxation in the mesothermal spectra. In 2005, Isupov [78] summarized the dielectric spectrum of a single crystal of BNT with temperature, and concluded that at 200 °C, a phase transition from FE to AFE appeared in BNT. The AFE to FE phase transition occurred near 320 °C, and the FE to paraelectric phase transition occurred at 540 °C. In 2010, Kling *et al.* and Hinterstein *et al.* proposed that the so-called ‘antiferroelectric phase’ was actually a non-polar phase [79–81], and further proved that the non-polar phase was a tetragonal phase (P4bm) structure through *in-situ* neutron diffraction and *in-situ* transmission electron microscope (TEM). With an increase in the applied electric field, the non-polar phase (P4bm) became the polar phase (R3c). At the same time, these two structures existed in the form of PNRs, which resulted in the relaxation of the system. This view was proved by Schmitt and Kleebe by selective electron diffraction and by Dorcet *et al.* [82, 83] using TEM. Using selective electron diffraction, Schmitt and Kleebe [82] thought that there was a strong  $1/2\{00e\}$  superlattice diffraction spot in region A, which was a uniform nanostructure that indicated a tetragonal phase in the structure (P4bm). In region B, with a thin-layer structure, there was a strong  $1/2\{00o\}$  superlattice diffraction spot, which indicated that the structure was in a rhombohedral phase (R3c). Upon examining the  $[011]_c$ ,  $[111]_c$ , and  $[013]_c$  zone axes of both regions A and region B, a  $1/2\{00o\}$  superlattice diffraction spot was observed in the  $[011]_c$  zone axis, indicating a tripartite phase (R3c). In the  $[111]_c$  zone axis, a  $1/2\{00e\}$  superlattice diffraction spot was observed, indicating a tetragonal phase (P4bm), while in the  $[013]_c$  zone axis,  $1/2\{00e\}$  and  $1/2\{00o\}$  superlattice diffraction spots coexisted. Moreover, it was also found that at each temperature point within the temperature range studied, two kinds of superlattice diffraction spot appeared, which told us that R3c and P4bm coexisted in this temperature segment.

Liu *et al.* [84, 85] investigated the phase evolution of a BNT– $K_{0.5}Na_{0.5}NbO_3$  (KNN) system which is summarized in figure 6. A combination of high-resolution synchrotron powder diffraction, neutron powder diffraction, and selected area electron diffraction was adopted. Two lead-free piezoelectric materials, BNT and KNN form an infinite substitution solid solution. Orthorhombic, tetragonal, and rhombohedral structures, and the phase-coexistence of orthorhombic and

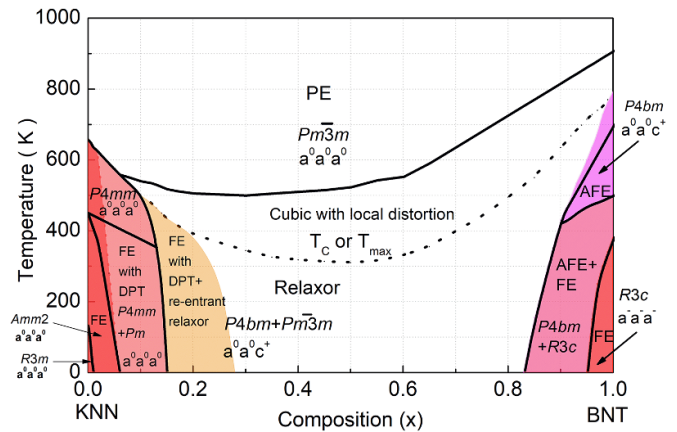


**Figure 6.** Phase diagram of the BNT–KNN system. Reprinted from [85], Copyright (2017), with permission from Elsevier.

tetragonal in  $0.02 < x \leq 0.14$ , tetragonal and pseudocubic in  $0.14 < x \leq 0.87$  and tetragonal and rhombohedral structures in  $0.87 < x \leq 0.96$ , were confirmed by subtle changes in the structures observed. The oxygen octahedral tilt systems  $a^0a^0a^+$  and  $a^-a^-a^-$  appear successively with an increase of BNT. The results indicated that KNN–BNT does not display an MPB similar to that of lead zirconate titanate. Four separate phase boundaries can be found in the phase diagram at room temperature; however, the phase-coexistence regions ( $0.02 < x < 0.14$  and  $0.87 < x < 0.96$ ) between phase boundaries should be described as a polycrystalline phase boundary rather than an MPB. A phase diagram was established, showing the relation between the dielectric permittivity measurements and the structural analyses. The local structure maintains distortions away from the cubic average structure in the range  $0.10 \leq x \leq 0.90$ . No clear correspondence with the temperature of the phase transition exists between the structural factors and the physical properties. The average lattice symmetry changes as follows: orthorhombic ( $x \sim 0.005$ )  $\rightarrow$  tetragonal ( $x \sim 0.10$ )  $\rightarrow$  pseudocubic ( $0.10 < x < 0.90$ )  $\rightarrow$  rhombohedral ( $x \geq 0.90$ ). With increasing BNT contents, the change in dielectric behavior follows the following sequence: normal FE  $\rightarrow$  diffuse-phase transition  $\rightarrow$  re-entrant-like relaxor  $\rightarrow$  relaxor + dipolar-glass-like relaxor  $\rightarrow$  BNT-like relaxor. The results were mainly elucidated by the nanoclusters and the disorder-driven nucleation of polar nanoregions contributed by a valence mismatch at one of the cation sites.

Using transmission electron microscopy and regional electron diffraction of BNT–BT–KNN ceramics at different temperatures, as described in figure 7, Dorcet *et al.* [83] found that the rhombohedral phase and the tetragonal phase coexisted in the grain of BNT ceramics. With an increase in temperature, the diffraction spot representing the tetragonal phase gradually increased, and the spot representing the rhombohedral phase gradually weakened. However, the spots representing the two phases were always observable in the range of 200 °C–320 °C. It was shown that the two structures coexisted in the form of PNRs over a wide temperature range of 200 °C–320 °C. In this way, a double peak dielectric spectrum with

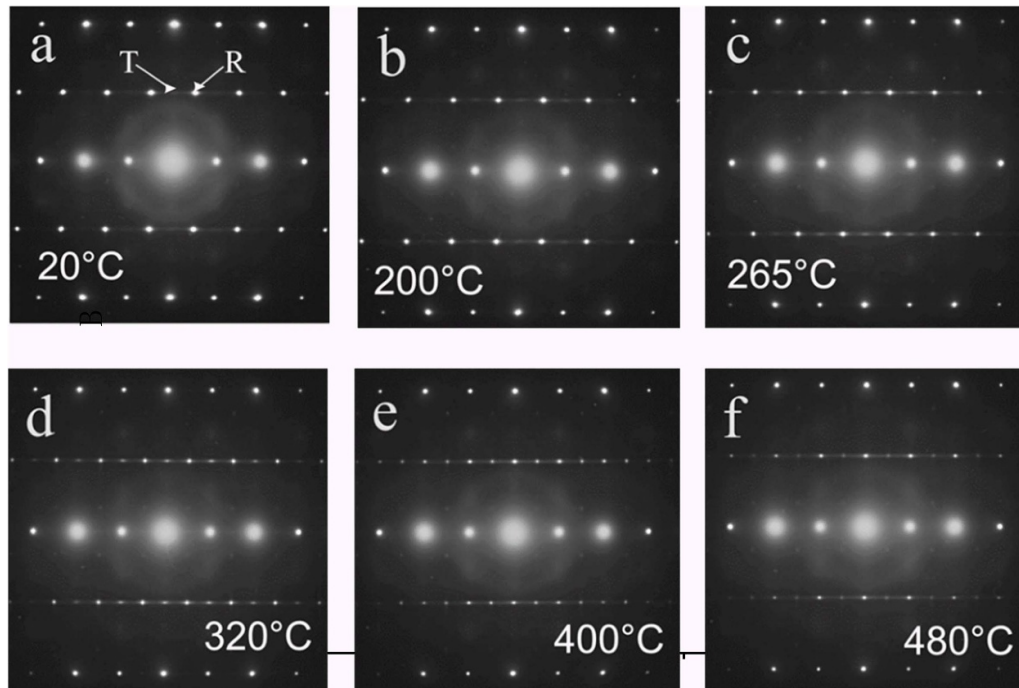


**Figure 7.** Electron diffraction patterns of BNT ceramics at different temperatures. Reprinted with permission from [83]. Copyright (2008) American Chemical Society.

temperature and the hysteresis loop at the beam waist were formed.

A growing number of researchers have subsequently carried out numerous studies to understand the relation between the fine phase structure and the FE behavior. Tai *et al* [86] studied the relationship between domain structure and temperature in BNT-based ceramics. It was found that there was no AFE long-range domain structure, so there was no transition between the FE phase and the AFE phase. By further studying the BNT–BT crystal structure, they concluded that the phenomenon similar to a double hysteresis loop was caused by the tilted octahedron formed by Ti and O at the B center site of the crystal structure, which resulted in a domain transformation. At the same time, Jo *et al* [87] studied the mesothermal spectra of BNT–BT and concluded that the anomalous points in the mesothermal spectra in the low-temperature range were not caused by the phase transition between the FE phase and the AFE phase but by the mutual transition between the R3c phase and the P4bm phase in the thermally activated polar domain. Viola *et al* [88] also studied the relationship between the phase structure and the temperature of BNT ceramics, and concluded that the abnormal points and double hysteresis loops of BNT ceramics were caused by a weakening of the Bi–O bond induced by temperature in the crystal structure, as well as the transformation between the non-polar phase and the polar phase induced by an applied electric field. The definition of BNT-based ceramics as relaxation FEs had been widely accepted by researchers. Using *in-situ* TEM, it was confirmed that the rhombohedral and tetragonal nanorods of BNT-based ceramics were combined in the cubic phase over an expansive temperature range.

Because the phase transition over a broad range of temperatures means that the two structures coexist over a wide temperature range in the form of PNRs, the free energy profile of polarization is generally flattened. Meanwhile, the energy barrier between the two phases is expected to be low. Under the same applied electric field, smaller PNRs can move more easily. Therefore, a small  $P_r$  and a hysteresis loop with a beam waist can be obtained. In addition, we find that slim  $P$ – $E$  loops with a small  $P_r$  value and a high  $P_{max}$  are responsible for the high energy density and efficiency. Small PNRs that coexist in BNT can lead to small  $P_r$  and are beneficial in obtaining large energy-storage density and efficiency. Hence, the dielectric dispersion and double hysteresis loop of BNT over a wide temperature range have attracted widespread attention.

In addition, the high-temperature relaxor phase between 200 °C and 320 °C was believed to have an AFE P4bm structure due to the distorted cubic phase caused by the in-phase rotation of the  $\text{TiO}_6$  octahedron about the  $c$  axis, as well as by the anti-parallel displacement of the cation along the polar  $c$  axis. The corresponding beam-waist AFE hysteresis loop with high polarization is considered to be very suitable for energy storage [89–91]. In 2011, the energy storage performance of a BNT–BT–KNN ceramic was reported at a medium electric-field strength of 50 ~ 60  $\text{kV cm}^{-1}$ . Thus, it has been considered by many researchers to be the most likely candidate to replace lead-based energy-storage materials [92–97]. BNT has a high Curie temperature. It can be used in high-temperature capacitors, and its high dielectric polarization is suitable for obtaining a high energy density [98]. Unfortunately, the remanent polarization  $P_r$  is not small enough, resulting in low efficiency in the processes of charging and discharging [99–101]. At room temperature, there is a



large coercive field ( $E_c = 73 \text{ kV cm}^{-1}$ ) [6, 102, 103], which makes BNT-based materials difficult to polarize. In addition, the sintering temperature required is fairly high ( $>1200 \text{ }^\circ\text{C}$ ) [100, 101] and  $\text{Bi}^{3+}$  and  $\text{Na}^+$  are easy to volatilize during the sintering process. Moreover, the conductivity is high and the dielectric loss is large. These factors lead to a large leakage current and a low breakdown strength of BNT-based dielectric ceramics [104].

### 3.1.2. Enhancement of energy storage properties.

Recently, many studies have focussed on improving the energy storage properties of BNT-based dielectric ceramics. For instance, BNT is usually modified by doping the second or multiple optimized phases. The main method of doping is to add perovskite materials with another phase. High breakdown-strength materials with a large energy gap, such as ST, CT, etc, were usually introduced to stabilize the structure and to increase the insulation. Furthermore, it was supposed that the dielectric permittivity of a solid solution would have good stability at high temperatures, and would therefore be very suitable for high-temperature capacitors. By introducing ST into BNT ceramics, Cao *et al* [105] discovered a hysteresis loop that was similar to that of an AFE when the ST content was 30%. Under an electric field of  $65 \text{ kV cm}^{-1}$ , an effective energy density of  $0.65 \text{ J cm}^{-3}$  was obtained, and the energy-storage performance was stable from room temperature to  $120 \text{ }^\circ\text{C}$ . The addition of ST increased the breakdown strength. When the addition of ST was 30 mol%, the temperature  $T_d$  (which represents the difference between FE and AFE) increased. In addition, strongly polarized materials such as AN, NN, BF, BT, etc, were usually adopted to increase  $P_{\text{max}}$ . In BNT–BT ceramics, Li *et al* [106] found that the hysteresis loop of ceramics was transformed into a waist-like double hysteresis loop, which resulted in a high  $W_{\text{rec}}$  of  $1.76 \text{ J cm}^{-3}$ . By doping BT,  $P_{\text{max}}$  obtained an obvious increase. The number of PNRs also increased, and therefore  $P_r$  decreased. Qi and Zuo [91] prepared an AFE ceramic with high energy storage, as well as temperature and frequency stability. By introducing NN into BNT, the highest effective energy density obtained was as high as  $7.02 \text{ J cm}^{-3}$ . Over a frequency range of 0.1–100 Hz,  $W_{\text{rec}}$  was also higher than  $3.50 \text{ J cm}^{-3}$  from  $25 \text{ }^\circ\text{C}$  to  $150 \text{ }^\circ\text{C}$ , and the fluctuation was less than 10%. The addition of NN increased  $P_{\text{max}}$ , decreased  $P_r$ , and strongly enhanced the energy storage properties of BNT. When ST, BT,  $\text{Bi}_{0.5}\text{K}_{0.5}\text{TiO}_3$  (BKT), and  $\text{Ba}_{0.85}\text{Ca}_{0.15}\text{Ti}_{0.9}\text{Zr}_{0.1}\text{O}_3$  were added to modify BNT, it was expected that an MPB would be formed due to the coexistence of the rhombohedral and tetragonal phases at room temperature. The general flattening of free energy at the MPB meant that the domain walls could move easily. Hence, the large  $P_r$  of BNT could be reduced. Chen *et al* [107] found that in  $(1-x)\text{BNT} - x\text{BT}$ , when the doping amount of Ba reached 0.06, its components were near the MPB. At this point, the maximum polarization of BNT–BT could reach  $35 \mu\text{C cm}^{-2}$ . However, due to the large coercive field and the large energy loss caused by domain inversion, the resulting BNT–BT was hardly usable. When BKT was added into 0.94BNT–0.06BT, Chandrasekhar and

Kumar [99] found that the effective energy density increased from  $0.485$  to  $0.598 \text{ J cm}^{-3}$  under an applied electric field of  $50 \text{ kV cm}^{-1}$ . Hence, a third group was also usually introduced, such as  $\text{CaZrO}_3$ ,  $\text{BaZrO}_3$ , KNN,  $\text{Bi}(\text{Mg}_{1/2}\text{Ti}_{1/2})\text{O}_3$ , etc. As a result, ternary BNT-based lead-free materials were obtained which caused a more disordered ionic competition, structural diversity, and charge mismatch. Furthermore, through the non-equivalent doping of the A-site and the B-site, not only was the energy loss decreased but also  $P_r$  was enhanced. Liu *et al* [108] investigated the effect of the addition of KNN on the FE and dielectric behaviors of the 90BNT–10ST system. Hysteresis loops indicated that a relaxor-AFE coherence was produced with the addition of KNN as a replacement for ST at up to 5at%. The 50BNT–50KNN presented a pure perovskite structure with pseudocubic symmetry based on synchrotron x-ray diffraction. However, superlattice reflections were observed by selected area electron diffraction and completely attributed to tetragonal P4bm in the neutron diffraction pattern. The relaxor behavior of 50BNT–50KNN was compared to those of Pb-based and Ba-based relaxors and discussed in the framework of the Vogel–Fulcher law and the new glass model. The 50BNT–50KNN ceramic behaved as a weak coupling relaxor with the strongest dielectric dispersion among them [109]. The correspondence between the temperature dependence of the phase structures and the experimental physical properties was made clear for the first time in the 90BNT–5ST–5KNN system by *in-situ* XRD, and *in-situ* Raman and impedance spectroscopy. Three consecutive events were identified by the relaxation time of electric modulus spectra and by deconvolving the temperature dependence of the dielectric permittivity using a phenomenological model. It was proposed that at room temperature, 90BNT–5ST–5KNN had a pseudocubic symmetry with rhombohedral R3c PNRs, that the mid-temperature local maximum in the temperature-dependent dielectric permittivity arose from a phase transition from R3c to P4bm, and that the high-temperature dielectric anomaly was associated with the thermal evolution of P4bm PNRs.

Doping with small amounts of rare-earth elements is another popular approach. Not only can the number of PNRs be increased, but also the different ionic valence can introduce donor/acceptor defects into the materials. Optimal concentrations of donor/acceptor doping defects can combine with conductive carriers, such as electrons and holes to form defect dipoles, which reduce the conductivity and ultimately reduce the dielectric loss at high temperatures. Moreover, rare-earth elements can improve the dielectric properties and inhibit the growth of grains. Borkar *et al* [110] studied the effect of a small amount of  $\text{Al}^{3+}$  doping on the structure and performance of BNT–BT. It was found that doping BNT–BT with a small amount of  $\text{Al}^{3+}$ , which is at the MPB, contributed to the formation of short-range ordered PNRs in the AFE phase. This also means that doping at different ionic radii and valences is beneficial to the formation of polar nanodomains. The ‘waist’ hysteresis loop can be observed from room temperature to  $100 \text{ }^\circ\text{C}$ , which confirms the coexistence of the relaxor phase and the AFE phase in BNT. Meanwhile, at  $50 \text{ kV cm}^{-1}$ , the material exhibited an energy storage density of  $0.4 \sim 0.6 \text{ J cm}^{-3}$  and a leakage diversion as low as  $1 \mu\text{A}$ . Xu *et al* [111] studied

the AFE property of 0.94BNT–0.06BT by doping it with Ta, and found that Ta doping can effectively reduce the remanent polarization, enhance the breakdown strength, and stabilize the AFE phase with a tetragonal structure. Hence, the 0.94BNT–0.06BT showed the phenomenon of a double hysteresis loop, similar to that of AFE. Under conditions of 60 °C and 70 kV cm<sup>-1</sup>, a  $W_{\text{rec}}$  of 0.94 J cm<sup>-3</sup> was obtained by doping the 0.94BNT–0.06BT with 2 mol% Ta. The introduction of Ta shifted the low-temperature dielectric anomaly to a lower temperature, while the high-temperature dielectric anomaly became broader. The dielectric relaxation was related to the dependence of the migration of oxygen vacancies and cation vacancies on the concentration of Ta. In addition, Li<sup>+</sup>, with a small radius (0.090 nm), was expected to co-substitute with Sr<sup>2+</sup> [112]. It was believed that Sr<sup>2+</sup> was introduced into the BNT perovskite structure to break the long-range domains, thereby generating PNRs in the matrix, and creating a path for relaxor behavior. Li<sup>+</sup> can lead to a distortion of the octahedral [TiO<sub>6</sub>] in the lattice, enhancing the  $P_{\text{max}}$  [113]. Finally, Sr<sub>x</sub>(Bi<sub>1-x</sub>Na<sub>0.97-x</sub>Li<sub>0.03</sub>)<sub>0.5</sub>TiO<sub>3</sub> bulk ceramics exhibited a large energy-storage capacity.

Furthermore, by doping highly polarizable materials, energy storage is also increased. Xu *et al* [101] introduced an NN terminal element into a BNT–BT solid solution. On the one hand, the effective energy density of BNT–BT increased (the energy-storage density was 0.71 J cm<sup>-3</sup> at a field strength of 70 kV cm<sup>-1</sup>). On the other hand, it presented good temperature stability in the temperature range of 25 ~ 150 °C (the change rate of energy-storage density was less than 12%). Mishra *et al* [114] prepared a BNT–BT–BF ternary ceramic system using plasma-activated sintering; the  $W_{\text{rec}}$  of this material achieved 1.4 J cm<sup>-3</sup> and the energy-storage efficiency was increased to 90%. Chen and Chu [42] found that the temperature range of BNT-based ceramics between the depolarization temperature and the Curie temperature (the temperature range between  $T_{\text{d}}$  and  $T_{\text{m}}$ ) could be extended by adding Bi(Mg<sub>0.5</sub>Ti<sub>0.5</sub>)O<sub>3</sub> (BMT). By doing so, the ceramic material had a small change in energy-storage performance over a wide temperature range. Compared with the undoped materials, 0.92BNT–0.08BT ceramics doped with BMT had a high  $W_{\text{rec}}$  (>2 J cm<sup>-3</sup>) at room temperature. At 120 °C, they presented a high energy storage efficiency (>88%), and the dielectric permittivity changed little between 100 °C and 400 °C. At the same time, they showed good temperature stability. In our group, Ma *et al* [115] introduced AN to substitute into the RFE 0.76BNT–0.24ST of MPB composition. A large recoverable energy-storage density of 2.03 J cm<sup>-3</sup> was obtained in BNT–ST–5AN ceramics under a small electric field of 120 kV cm<sup>-1</sup>, which was superior to that of other lead-free energy-storage materials under similar electric fields.

In addition to the above, BNT has great potential to increase the operating temperature, increase the capacity, and reduce the volume of multilayer ceramic capacitors. Moreover, the Curie temperature of BNT is relatively high, up to  $T_{\text{c}} = 520$  °C, and it is not sensitive to the sintering atmosphere and environmental humidity. Hence, the preparation process has good repeatability. However, there are also several disadvantages: (a) the volatilization of Bi<sup>3+</sup> during

the sintering process makes it easy to produce oxygen vacancies and other defects, which lead to an increase in the high-temperature conductivity and a decrease in insulation. (b) The dielectric loss is large at high temperatures. (c) The large remanent polarization  $P_{\text{r}}$  is not beneficial for high energy-storage efficiency. (d) The sintering temperature range is narrow, etc.

### 3.2. BiFeO<sub>3</sub>-based ceramics

In the 1950s, BF received widespread attention as a multi-ferroic material due to the high polarization of Bi<sup>3+</sup> and the anti-ferromagnetism of Fe<sup>3+</sup>. Due to the volatility of Bi at high temperatures, there were too many oxygen vacancies with conductivity, and Fe<sup>3+</sup> was easy to change into Fe<sup>2+</sup>. These factors led to a large leakage current and the failure to synthesize a high-quality BF sample. This was the reason for the small progress in the research into the FE properties of BF [116]. In 1970, Teague *et al* [117] measured the intrinsic FE polarization along the pseudocube [001] direction, which was once thought to be only 3.5 μC cm<sup>-2</sup> and found an FE polarization along the [111] direction of only 6.1 μC cm<sup>-2</sup>. Smolenskii *et al*'s research group [118] then studied this material, and believed that the failure of the polarization curve which could not reach the saturation value could be attributed to the poor quality of single crystals or ceramics, as well as the high conductivity caused by oxygen vacancies. Meanwhile, the mixed valence of Fe also made the measurement of the intrinsic electrical properties elusive. However, in 1975, Kaczmarek *et al* [119] observed that the Curie temperature of BF FE might be as high as 1103 K, and neutron diffraction, x-ray technology and first-principles calculations all showed that Bi, Fe and O atoms in the crystal had a relative displacement along the triple symmetry axis. In perovskites, Bi and O have a strong displacement relative to the pseudo-cubic center of perovskites, and the FE phase-transition temperature is high. Hence, researchers began to query the small 'intrinsic' FE property. In the following years, a series of electrical measurements of bulk samples always supported a small value for FE polarization in BF. For example, Kumar *et al* [120] observed an FE polarization of 8.9 μC cm<sup>-2</sup> in bulk ceramics. They believed that the reason for this phenomenon was the poor crystal quality, which hindered the accurate measurement of saturation polarization. Usually, the intrinsic polarization value of BF is minimal in the rhombohedral phase, and so it is only possible to achieve large FE polarization by lattice distortion. In addition, the polarization does not depend on a single lattice vector. According to modern polarization theory, different polarization flipping and other factors can also provide different FE polarization values. Neaton *et al* [121, 122] calculated that the FE polarization value of BF was 50 ~ 90 μC cm<sup>-2</sup> from first principles, and theoretically predicted the existence of the intrinsic large FE polarization for the first time. Together with the research into BF thin-film materials by Ramesh's research group [123] in 2003 and research into BF high-quality single crystals by the group of Lebeugle *et al* [124] in 2007, these studies were the prelude to new research and to the modern

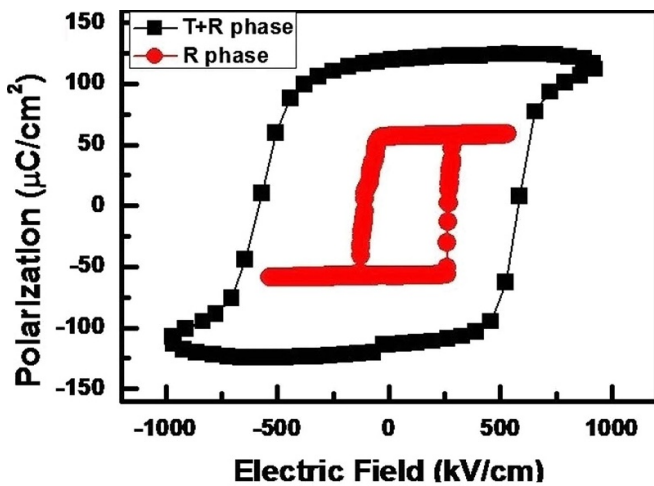


**Figure 8.** FE hysteresis loops of rhombohedral- and tetragonal-phase BF, indicating the existence of strong FE polarization. Reprinted (figure) with permission from [126], Copyright (2011) by the American Physical Society.

understanding of the FE properties of BF. The main polarization sequence of the rhombohedral BF crystal is along the [111] direction, and the polarization of the [111] oriented film is theoretically predicted to be  $100 \mu\text{C cm}^{-2}$ . Yun *et al* [125] even predicted that the spontaneous FE polarization of BF could be as high as  $150 \mu\text{C cm}^{-2}$ , based on its huge lattice constant ( $c/a = 1.25$ ), which was called the ‘super tetragonal’ structure. By measuring the direct hysteresis loop of the pure tetragonal-phase BF, Hang *et al* [126] found that the spontaneous polarization of BF could reach more than  $140 \mu\text{C cm}^{-2}$ , which experimentally proved the existence of strong polarization in BF, as shown in figure 8.

Since the polarization can be as high as  $100 \mu\text{C cm}^{-2}$ , BF is considered to have a large  $P_{\text{max}}$  and to offer an enormous potential energy-storage density [127]. In addition, the high Curie temperature of  $830 \text{ }^\circ\text{C}$  is very suitable for high-temperature capacitance for energy storage. Hence, BF has been greatly discussed in the field of energy storage. In Nd-modified  $\text{Bi}_{1-x}\text{R}_x\text{FeO}_3$  systems, Xu *et al* [128] even theoretically predicted it could potentially allow a high energy density ( $100\text{--}150 \text{ J cm}^{-3}$ ) and efficiency ( $80\%\text{--}88\%$ ) for electric fields which may be within the range of feasibility following experimental advances ( $20\text{--}30 \text{ kV cm}^{-1}$ ). Calisir *et al* [129] observed a double hysteresis loop with a waist beam and obtained an effective energy density of  $0.61 \text{ J cm}^{-3}$  in  $0.75\text{BF}\text{--}0.25(\text{Ba}_{0.99}\text{La}_{0.01})\text{TiO}_3$  ceramics. However, it is obvious that the large remanent polarization  $P_r$  is not suitable for energy storage. A second or third component, such as BT, ST, BNT, etc., was usually introduced to decrease  $P_r$ , and the resulting material has been reported to show RFE-like features. BT and ST have even been introduced to break the long-range domains so that the general flattening of the free energy profile is beneficial to the movement of PNRs [130]. At the same time, BT and ST can effectively suppress the appearance of the impurity phase and the volatilization of Bi [131, 132]. A BF–ST thin film was reported to have a good energy-storage

density of  $18.6 \text{ J cm}^{-3}$  at  $972 \text{ kV cm}^{-1}$  [133]. In the BF–BT system,  $0.67\text{BF}\text{--}0.33\text{BT}$  was believed to have a high  $P_{\text{max}}$  with a rhombohedral to pseudocubic structural phase boundary [134, 135]. However, the energy loss is too large, due to the large  $P_r$ , and the energy density is not desirable due to the low breakdown strength. By introducing ST,  $\text{Ba}(\text{Mg}_{1/3}\text{Nb}_{2/3})\text{O}_3$ ,  $\text{Sr}(\text{Al}_{0.5}\text{Nb}_{0.5})\text{O}_3$ , etc., as ternary, a high energy storage capacity is obtained. For example, in BF–BT–ST, though  $P_{\text{max}}$  decreased,  $P_r$  also rapidly decreased. As a result, a decrease in the domain size from 5 to 2 nm was clearly observed [130]. Liu *et al* [136] obtained a  $W_{\text{rec}}$  of  $2.56 \text{ J cm}^{-3}$  at  $160 \text{ kV cm}^{-1}$  using  $\text{Ba}(\text{Zn}_{1/3}\text{Ta}_{2/3})\text{O}_3$ -doped BF–BT. Energy storage values of  $1.56 \text{ J cm}^{-3}$  at  $125 \text{ kV cm}^{-1}$  [137] and  $1.75 \text{ J cm}^{-3}$  at  $155 \text{ kV cm}^{-1}$  [138] were also achieved in  $\text{Sr}(\text{Al}_{0.5}\text{Nb}_{0.5})\text{O}_3$ - and  $\text{Ba}(\text{Mg}_{1/3}\text{Nb}_{2/3})\text{O}_3$ -modified BF–BT ceramics. In addition, it was reported that by replacing Bi with the rare-earth elements La, Nd, Sm, etc., it was effectively possible to enhance the energy storage properties of  $0.67\text{BF}\text{--}0.33\text{BT}$  ceramics. Calisir *et al* [129] obtained a  $W_{\text{rec}}$  of  $0.61 \text{ J cm}^{-3}$  at  $10 \text{ kV cm}^{-1}$  in La-modified  $0.75\text{BF}\text{--}0.25\text{BT}$  ceramics. Wang *et al* [139] obtained  $1.82 \text{ J cm}^{-3}$  at  $180 \text{ kV cm}^{-1}$  with Nd-doped  $0.75\text{BF}\text{--}0.25\text{BT}$ . Furthermore, Fujino *et al* [140] found an MPB in  $\text{Bi}_{0.86}\text{Sm}_{0.14}\text{FeO}_3$  ceramics, which had a pseudocubic–orthorhombic (FE to AFE) transition, and it achieved a superior energy-storage performance in Sm-Modified  $0.67\text{BF}\text{--}0.33\text{BT}$  ceramics. In addition to the large  $P_r$ , the moderate bandgap and the poor insulation are the other major issues that significantly restrict the application of BF-based ceramics in energy storage. By doping a  $0.67\text{BF}\text{--}0.33\text{Ba}_{0.8}\text{Sr}_{0.2}\text{TiO}_3$  ceramic with the sintering aid  $\text{MnO}_2$ , the grain size was refined and the insulation was increased. Moreover, the higher-valence Mn inhibited the change of  $\text{Fe}^{3+}$  to  $\text{Fe}^{2+}$ . It is believed that, in the sintering process, higher-valence Mn ions can absorb electrons when they evolve into lower-valence  $\text{Mn}^{3+}$  and  $\text{Mn}^{2+}$  ions, thereby inhibiting the change from  $\text{Fe}^{3+}$  to  $\text{Fe}^{2+}$ . Hence, the insulation could be enhanced [141]. In other words, in the field of energy storage, several BF weaknesses need to be overcome. Firstly, the large  $P_r$  is not suitable for energy storage, and it leads to low energy-storage efficiency. Secondly, the volatilization of Bi, the easy formation of the Bi-rich phase and the change of  $\text{Fe}^{3+}$  to  $\text{Fe}^{2+}$  can also cause many unwanted effects, such as too many defects, large leakage currents, low breakdown strength, poor insulation, etc.

On the other hand, due to the high electrical polarizability of BF, it is often used to improve the maximum polarization  $P_{\text{max}}$  so as to improve the energy storage density. Wang *et al* [142] obtained an effective energy density  $W_{\text{rec}} = 10.5 \text{ J cm}^{-3}$  in BF–BT multilayer ceramics. It was supposed that the doping of BF had increased the  $P_{\text{max}}$  greatly. At the same time, with a larger number of PNRs compared to pure BT, the charge–discharge efficiency  $\eta$  reached 87%, a sharp increase. Furthermore, due to the high Curie temperature of BF, the temperature coefficient was more stable, and the rate of capacitance changed by less than 15% within the temperature range of  $25 \text{ }^\circ\text{C}\text{--}150 \text{ }^\circ\text{C}$ , which easily met the X9R standard for capacitance. Chen *et al* [143] obtained an energy-storage density  $W_{\text{rec}} = 2.8 \text{ J cm}^{-3}$  and an energy-storage



efficiency  $\eta = 55.8\%$  in the  $0.67\text{Bi}_{1-x}\text{Sm}_x\text{FeO}_3\text{-}0.33\text{BT}$  system. Other Bi-based materials, such as BMT,  $\text{Bi}(\text{Zn}_{0.5}\text{Zr}_{0.5})\text{O}_3$  (BZZ),  $\text{Bi}(\text{Zn}_{0.5}\text{Sn}_{0.5})\text{O}_3$  (BZS), etc, are also often added to increase  $P_{\max}$ . The maximum polarization  $P_{\max}$  of these systems is improved, and the FE long-range domains are broken into polar nanodomains due to the disorder of the A- and B-sites, lattice mismatch, ionic disorder, etc. Zhou *et al* [144] doped BT with BZS, and increased the energy storage density of BT to  $2.41 \text{ J cm}^{-3}$ . The corresponding energy-storage efficiency increased to 91.6%. Moreover, the energy-storage performance of the BT–BZS system showed excellent temperature stability ( $20 \sim 160 \text{ }^\circ\text{C}$ ), frequency stability ( $1 \sim 1000 \text{ Hz}$ ), and fatigue stability ( $10^5$  cycles), which meet the requirements for an X8R capacitor very well. They also pointed out that the structural differences between BT and BZS lead to a weak-coupling relaxation between the polar nanodomains, which enables them to respond rapidly to the applied electric field. Similar results were found for NN doped with BZZ by Zhou *et al* [145]. For the NN–BZZ system, the energy-storage density was  $3.14 \text{ J cm}^{-3}$  and the highest energy-storage efficiency was (84.5%). Moreover, the energy-storage characteristics showed excellent temperature stability ( $20 \sim 160 \text{ }^\circ\text{C}$ ), frequency stability ( $1 \sim 1000 \text{ Hz}$ ) and fatigue ( $10^5$  cycles) stability (<2%). Zhou *et al* [146] found that a  $0.835(\text{Na}_{0.5}\text{Bi}_{0.5})\text{TiO}_3\text{-}0.05\text{BT}\text{-}0.125\text{Bi}(\text{Zn}_{2/3}\text{Nb}_{1/3})\text{O}_3$  (0.835BNT–0.05BT–0.125BZN) ceramic exhibited a high energy storage density of  $\sim 4.23 \text{ J cm}^{-3}$ , a discharged energy density of  $\sim 2.83 \text{ J cm}^{-3}$  and an efficiency of  $\sim 67\%$  under a relatively low electric field of  $180 \text{ kV cm}^{-1}$ . By introducing BZN, compared with BNT–BT, the grain of the 0.835BNT–0.05BT–0.125BZN ceramic was refined and the energy density and stability were also improved. Yang *et al* [43] used BF to modify KNN, and found that a large  $W_{\text{rec}}$  of  $2 \text{ J cm}^{-3}$  was achieved in a  $0.9\text{KNN}\text{-}0.1\text{BF}$  ceramic at  $206 \text{ kV cm}^{-1}$ , which was superior to that of KNN under the same conductive conditions. Furthermore, the addition of BF increased the energy-storage efficiency  $\eta$  of KNN. Hu *et al* [147] used the solid-state route to prepare a  $0.88\text{BT}\text{-}0.12\text{BMT}$  ceramic; an energy storage of  $1.81 \text{ J cm}^{-3}$  was obtained at room temperature. In 2018, Yuan *et al* [63] prepared a  $0.88\text{BT}\text{-}0.12\text{BMT}$  FE ceramic using the traditional solid-state route; a discharge energy-storage density of  $2.9 \text{ J cm}^{-3}$  and an energy-storage efficiency of 86.8% were obtained simultaneously, due to the  $x = 0.15$  component. In addition, the energy-storage density and energy-storage efficiency were increased by 6.25 times and 1.56 times, respectively, compared to the undoped component, BT.

### 3.3. $\text{Sr}_{0.7}\text{Bi}_{0.2}\text{TiO}_3$ -based ceramics

$\text{Sr}_{0.7}\text{Bi}_{0.2}\text{TiO}_3$  (SBT) is an RFE material with a perovskite structure. The main structure of SBT is derived from ST, which has a simple cubic perovskite structure. As a paraelectric material, ST has a low dielectric permittivity, similar to that of other paraelectric materials. SBT is produced from ST doped with  $\text{Bi}^{3+}$  at the A-site, and the polarization  $P_{\max}$  of this system is further enhanced. SBT is an RFE. Its relaxor characteristics are derived from the vacancy of Sr and the off-central

migration of the Bi element [148], so SBT has a low  $P_r$  and coercive field, which contributes to a high  $\eta$  in energy-storage applications. However, the  $P_{\max}$  of SBT is still minimal, which has limited the application of SBT considerably in the field of energy storage [149]. SBT has plenty of advantages; for example, due to the defect vacancy of the Sr ion at the A-site and the volatilization of Bi during the sintering process, it has good FE relaxation and dielectric dispersion. The maximum permittivity is available over a wide temperature range. As the defect dipole is formed by an oxygen vacancy or A-site defect, the increase of PNRs caused by the different radius of Sr and Bi ions, as well as the electron polarization of the outermost  $6s^2$  electron layer of the  $\text{Bi}^{3+}$  ions, the polarization and dielectric permittivity of SBT are much larger than those of ST, and it has greater potential prospects for use in energy storage. Due to the increase of PNRs and its low coercive field, SBT has a higher energy-storage efficiency. Based on these advantages, SBT has attracted more and more attention in recent years.

Zhang *et al* [150] investigated the relaxation behavior of  $\text{Sr}_{(1-1.5x)}\text{Bi}_x\text{TiO}_3$  ceramics and reported an energy storage density of  $1.63 \text{ J cm}^{-3}$ , with an  $\eta$  of 61.4% at  $217.6 \text{ kV cm}^{-1}$ . Chao *et al* [151] reported that RFE ceramics (Sr, Pb, Bi) $\text{TiO}_3$  possess an energy storage density of  $0.228 \text{ J cm}^{-3}$  with an  $\eta$  of 94.2% at  $50 \text{ kV cm}^{-1}$ . However, the low breakdown strength of SBT-based ceramics has restricted the further improvement of their energy-storage performance. Zhao *et al* [152] introduced CT with a low dielectric loss and a high breakdown strength (up to  $4200 \text{ kV cm}^{-1}$ ) into SBT ceramics. Appropriate doping with Ca refined the grain, increased the breakdown strength from 239 to  $313 \text{ kV cm}^{-1}$ , and increased the energy-storage density to  $1.95 \text{ J cm}^{-3}$ . Ding [153] observed an energy-storage density as high as  $35 \text{ J cm}^{-3}$  in a thin film of  $0.5\text{BNT}\text{-}0.5\text{SBT}$ . The energy-storage efficiency was 73.8%, and the breakdown strength was up to  $3200 \text{ kV cm}^{-1}$  at room temperature. More importantly, the corresponding thin film showed superior thermal stability ( $20 \text{ }^\circ\text{C}\text{-}140 \text{ }^\circ\text{C}$ ), frequency stability ( $10^2\text{-}10^4 \text{ Hz}$ ), and fatigue endurance for long-term use ( $10^4$  cycles).

## 4. Problems and strategies

### 4.1. Problems in Bi-based energy storage ceramics

Similarly to  $\text{Pb}^{2+}$ , the lone pair of electrons in the outermost  $6s^2$  layer can be hybridized with the 6p vacant orbital or the  $\text{O}^{2-}$  orbital to produce strong electron cloud polarization. At the same time, Bi-based ceramics have been widely investigated in the field of FE energy storage [17]. Due to their high polarization and their potentially large energy-storage density, it is believed that these materials are among those most likely to replace Pb-based materials. However, many shortcomings are obvious. For example, in the process of sintering, it is easy to form a Bi-rich phase at high temperature, which produces a large leakage current and lowers the insulation. At the same time, the defects and oxygen vacancies caused by the volatilization of Bi can also lead to high conductivity, and then greatly reduced insulation, which decrease the energy storage properties. Although defective dipoles increase the



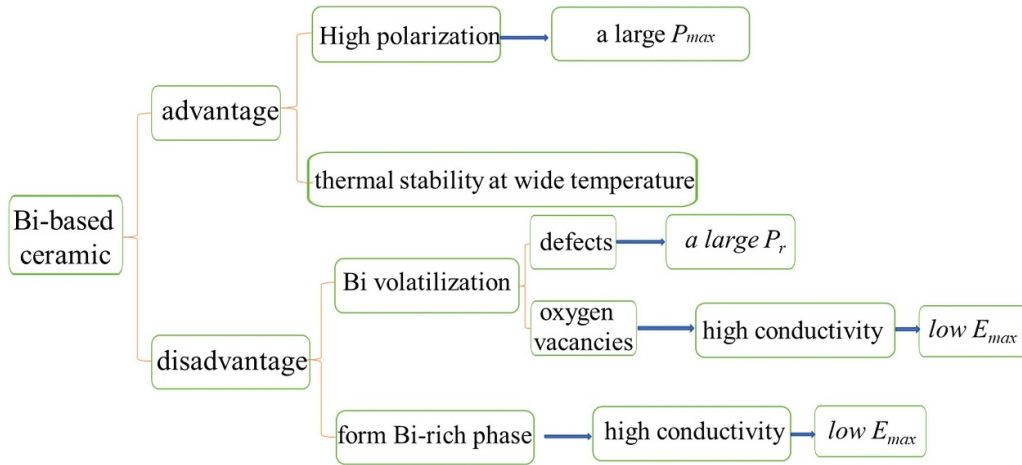


Figure 9. Advantages and disadvantages of Bi-based ceramics.

maximum polarization  $P_{max}$ , they also increase the remanent polarization  $P_r$ . Based on previous research, the advantages and disadvantages of Bi-based ceramics are summarized in figure 9.

In addition, we list the performances of some Bi-based energy-storage ceramics in table 1. It can be seen from table 1 that the energy storage of Bi-based ceramics is worse than that of Pb-based ceramics in terms of energy-storage density and energy-storage efficiency. Therefore, there is still a lot of work to be done to improve the energy storage performance of Bi-based ceramics. In order to reduce Bi volatilization and the formation of the Bi-rich phase, some common methods, such as powder-embedded sintering, low-temperature sintering, flash sintering, and liquid-phase sintering are usually used. In addition, in recent years, many existing and new methods have been tried by previous researchers to improve the energy storage performance of Bi-based ceramics. We summarize and classify them in the following. At the same time, some non-Bi-based material methods have also been added, and we consider this a good reference for improving the energy storage performance of Bi-based ceramics.

## 4.2. Strategies and methods

**4.2.1. Chemical modification.** From current research, we find that chemical modification is usually adopted to enhance the energy storage properties. For example, high bandgap modification, high-polarization material modification, rare-earth element modification, non-stoichiometric chemical modification, etc, are usually used.

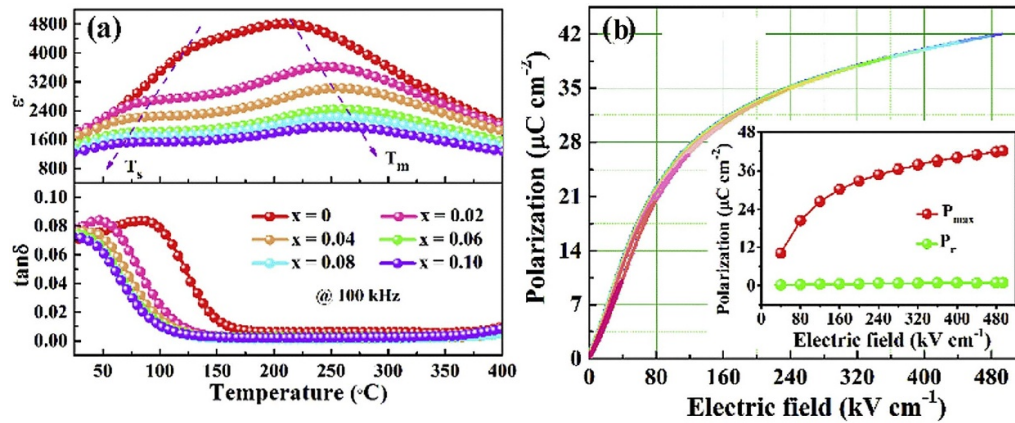
- (a) By doping linear dielectrics with high bandgap materials such as ST, CT, etc, the breakdown strength and insulation can clearly be increased, corresponding to improved energy-storage density and energy-storage efficiency. Generally, linear dielectrics with a high bandgap have high breakdown strength, low loss, and high energy storage efficiency. The upper limit of the breakdown strength of ST is  $16\ 000\ \text{kV cm}^{-1}$  [12, 58]. CT also has a high breakdown strength ( $>10\ 000\ \text{kV cm}^{-1}$ ) and a

Table 1. The energy-storage properties of some Bi-based ceramics.

Components	E (kV cm <sup>-1</sup> )	W <sub>rec</sub> (J cm <sup>-3</sup> )	η (%)	Ref.
BNT-ST	65	1.91	73.6	[105]
BNT-KNN	100	1.2	—	[106]
BNT-NN	390	7.02	85	[91]
BNT-BST-NN	116	1.25	76	[103]
BNT-NN-Ca	180	2.85	80	[9]
BNT-BT-NN	70	0.71	66	[101]
SBT-BMZ	380	4.2	88	[154]
BNT-BT-BMT	225	2	88	[155]
BNT-ST-NN	70	0.74	55	[156]
BNT-La-Zn	200	3.24	82	[157]
BNT-BST	100	1.04	77	[158]
BNT-ST-AN	120	2.03	—	[115]
SBT-BKT	220	2.21	91.4	[149]
SBT-Ca	290	2.1	97.6	[152]
BF-BT-AN	195	2.11	84	[52]
BF-KNN	206	2	63	[43]
BF-BST-LMN	230	3.38	59	[141]
BF-BT-BMN	125	1.56	75	[159]
BF-BT-Nd	90	0.71	—	[160]

BMZ—Bi(Mg<sub>0.5</sub>Zr<sub>0.5</sub>)O<sub>3</sub>, BMT—Bi(Mg<sub>0.5</sub>Ti<sub>0.5</sub>)O<sub>3</sub>, BKT—Bi<sub>0.5</sub>K<sub>0.5</sub>TiO<sub>3</sub>, AN—AgNbO<sub>3</sub>, KNN—K<sub>0.5</sub>Na<sub>0.5</sub>NbO<sub>3</sub>, ST—SrTiO<sub>3</sub>, BF—BiFeO<sub>3</sub>, BT—BaTiO<sub>3</sub>, SBT—Bi<sub>0.2</sub>Sr<sub>0.7</sub>TiO<sub>3</sub>, NN—NaNbO<sub>3</sub>, LMN—La(Mg<sub>2/3</sub>Nb<sub>1/3</sub>)O<sub>3</sub>, BMN—Bi(Mg<sub>0.5</sub>Nb<sub>0.5</sub>)O<sub>3</sub>, AN—AgNbO<sub>3</sub>.

temperature-independent energy-storage behavior. Hence, it is suitable for high-temperature applications [12, 57]. By introducing linear dielectric media, such as ST and CT, Sr and Ca can replace Bi, thereby reducing the influence of high conductivity and reducing the effects on breakdown strength caused by the volatilization of Bi. In addition, the different crystal lattices created by introducing ST etc, can also produce a large number of PNRs, which are beneficial to obtaining a small  $P_r$  and high energy efficiency. For BNT films modified with ST, Xu *et al* [161] found that ST greatly increased the breakdown strength, and moreover expanded the difference between  $P_{max}$  and  $P_r$ . An energy storage of  $36.1\ \text{J cm}^{-3}$  and an energy-storage efficiency of 40.8% were obtained in a 0.95BNT-0.05ST thin film.



**Figure 10.** (a) Temperature dependence of  $\epsilon'$  and  $\tan\delta$  of  $0.75\text{Na}_{(0.5-x)}\text{Bi}_{(0.5+x)}\text{TiO}_3-0.25\text{SrTiO}_3$  ceramics at 100 kHz; (b) unipolar  $P-E$  loops of BNST ceramics under different electric fields at 10 Hz and room temperature (inset shows the variation of  $P_{\max}$  and  $P_r$  under different electric fields) [165].

In a BKT system modified with ST, Shiga *et al* [162] found that ST greatly improved the temperature stability of BKT. In a  $\text{Sr}_{0.6}(\text{Na}_{0.5}\text{Bi}_{0.5})_{0.4}\text{Ti}_{0.99}\text{Mn}_{0.01}\text{O}_3$  thin film, Zhang *et al* [163] found that the addition of ST reduced the oxygen vacancies and increased the breakdown strength. An energy-storage density of  $33.58 \text{ J cm}^{-3}$  was obtained. Using ST doping, Cui *et al* [164] increased the breakdown strength of BNT to  $210 \text{ kV cm}^{-1}$  in a  $0.4\text{BNT}-0.6\text{ST}$  ceramic. Furthermore, the dielectric anomalies  $T_m$  are shifted to a higher temperature, and the discharge energy density is also increased.

- (b) Materials with strong polarization, such as AN, NN etc, have usually been introduced to increase  $P_{\max}$ , accompanied by a decrease in  $P_r$ , which can increase the energy storage density; examples are NN-modified BNT–BT [101], BF-modified BNT–BT [114], etc.
- (c) Replacing Bi with La, Nd, Sm, etc, rare-earth elements can effectively break the long-range domains into PNRs due to ion position competition, charge disorder, etc. For example, by introducing  $\text{Li}^+$ , the relaxor behavior of BNT was enhanced and the distortion of octahedral  $[\text{TiO}_6]$  in the lattice led to an increase of  $P_{\max}$  [113]. Doping with higher-valence Mn increased the insulation and decreased the leakage current by inhibiting the change of  $\text{Fe}^{3+}$  into  $\text{Fe}^{2+}$  etc [141].
- (d) By doping with a non stoichiometric chemical, such as SBT, etc, an increase in defect dipoles can increase  $P_{\max}$ . In addition, defect dipoles can reduce the conductivity, and ultimately reduce the dielectric loss of materials at high temperature. For example, by doping KBT with SBT, Zhao *et al* [149] found that the SBT greatly improved the breakdown strength and increased the energy storage efficiency. The energy-storage density of  $0.62\text{SBT}-0.38\text{KBT}$  ceramic is  $2.21 \text{ J cm}^{-3}$ , and its energy-storage efficiency is 91.4%. It also has excellent frequency stability (10 Hz–500 Hz), temperature stability ( $-55 \text{ }^\circ\text{C}$ – $150 \text{ }^\circ\text{C}$ ), and fatigue stability ( $1-10^5$ ). Yan *et al* [165] used A-site defect engineering to reduce the oxygen vacancies in BNT-based ceramics and inhibited the grain growth, as

shown in figure 10. In ceramics with a chemical composition of  $0.75\text{Na}_{(0.5-x)}\text{Bi}_{(0.5+x)}\text{TiO}_3-0.25\text{SrTiO}_3$ , the breakdown strength, energy-storage density, and energy-storage efficiency were significantly improved by controlling the Bi and Na contents. When the maximum electric field was  $535 \text{ kV cm}^{-1}$ , the energy-storage density reached  $5.63 \text{ J cm}^{-3}$  and the efficiency reached 94%. Meanwhile, A-site defect engineering has broadened the temperature stability of the dielectric permittivity in  $0.75\text{Na}_{(0.5-x)}\text{Bi}_{(0.5+x)}\text{TiO}_3-0.25\text{SrTiO}_3$  ceramic. In addition, the dielectric permittivity showed obvious dielectric relaxation over a wide temperature range from room temperature to  $100 \text{ }^\circ\text{C}$ .

- (e) In addition, MPBs and PNRs are usually discussed in energy storage. Correspondingly, composition design and domain engineering are also considered to be the main methods for increasing the performance of energy storage. Composition modification can drive the formation of a phase boundary [17]. An MPB is usually adopted, since it is considered to respond to many excellent properties, such as piezoelectricity, electro strain, energy storage, and electrocaloric etc. Near the components of the MPB, different crystal phases usually coexist. Different phase structures and ionic radii cause long-range domains to evolve into PNRs. In the transition region caused by domain walls and an MPB, the free energy profile of polarization is generally flattened. The energy barrier between two or more phases is expected to be low. Under the same applied electric field, small PNRs can move more easily. From previous research, at the MPB component,  $0.94\text{BNT}-0.06\text{BT}$ ,  $0.76\text{BNT}-0.24\text{ST}$ , etc, usually showed excellent energy-storage performance. In addition, the energy-storage property has been improved via domain design techniques such as texturization, low-temperature polarization, nanodomain engineering, etc. A large  $W_{\text{rec}}$  of  $70 \text{ J cm}^{-3}$  was achieved in BF–ST thin films through domain engineering [130]. In 2019, a large  $W_{\text{rec}}$  ( $8.12 \text{ J cm}^{-3}$ ), a high  $\eta$  (90%), and excellent thermal stability were simultaneously obtained

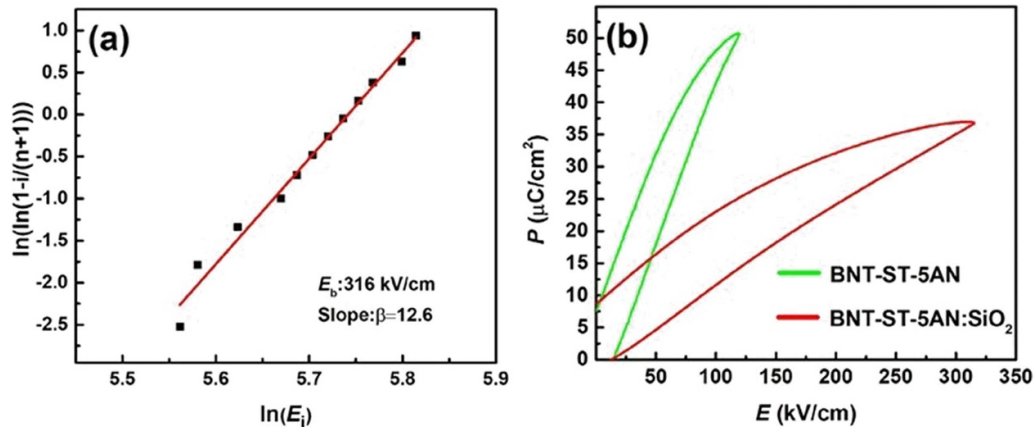


**Figure 11.** (a) Weibull distribution and statistical breakdown-strength calculation of BNT-ST-5AN:SiO<sub>2</sub>, (b) the  $P$ - $E$  loops of BNT-ST-5AN and composite ceramics at  $E_b$ . Reprinted from [104], Copyright (2019), with permission from Elsevier.

in a BF-BT-NN ceramic based on a significant improvement in the breakdown strength via nanodomain engineering [166].

**4.2.2. Refinement of grain.** Grain size is another important factor that affects the energy storage density of ceramics. Fine grain is beneficial for the formation of thin hysteresis loops, and also for improving the breakdown strength. In general, the relationship between the breakdown strength  $E_b$  and the grain size  $G$  is considered to be  $E_b \propto \frac{1}{\sqrt{G}}$ . This means a refined grain is required for high breakdown strength. The addition of a sintering aid or optimization of the sintering process is often adopted to refine the grains.

(a) In terms of adding a sintering aid, glass powder is usually considered. This is conducive to grain refinement, and can also increase the grain boundary energy. Meanwhile, it can increase the insulation of ceramics, and improve the breakdown strength [17]. Besides, the addition of glass powder and other sintering aids can reduce the existence of pores and improve the density of ceramics in the sintering process. Ma *et al* [104] successfully reduced the sintering temperature of 0.95(0.76BNT-0.24ST)-0.05AN RFE ceramics from 1150 °C to 980 °C by two-phase compounding with nano-sized SiO<sub>2</sub>. At the same time, the average grain size of the composite ceramic was also greatly reduced, from 4.45 to 0.37 μm. A large recoverable energy-storage density (3.22 J cm<sup>-3</sup>) was achieved, with ultrahigh breakdown strength (316 kV cm<sup>-1</sup>), as shown in figure 11. In non-Bi based materials, adding a sintering aid has also aided the performance in the past. Liu *et al* [167] added 3 wt.% SiO<sub>2</sub> into Ba<sub>0.3</sub>Sr<sub>0.7</sub>TiO<sub>3</sub> (BST). The breakdown strength of BST increased from 130 to 380 kV cm<sup>-1</sup>, and, compared with pure BST ceramics, the energy-storage density and efficiency increased by 3.3 times. By modifying Ba<sub>x</sub>Sr<sub>1-x</sub>TiO<sub>3</sub> with a glass made of B<sub>2</sub>O<sub>3</sub>-Bi<sub>2</sub>O<sub>3</sub>-SiO<sub>2</sub>-CaO-BaO-Al<sub>2</sub>O<sub>3</sub>-ZrO<sub>2</sub>, Shen *et al* [168] found that the dielectric loss of the ceramics could be strongly suppressed from  $\tan\delta > 20\%$  to  $\tan\delta < 3\%$ ,

and that the efficiency could reach 91.6%. Xiao *et al* [169] used BaO-B<sub>2</sub>O<sub>3</sub>-Al<sub>2</sub>O<sub>3</sub>-SiO<sub>2</sub> glass powder as an additive, and increased the energy storage density of Ba<sub>0.4</sub>Sr<sub>0.6</sub>TiO<sub>3</sub> from 1.74 to 3.1 J cm<sup>-3</sup>, an increase of 1.8 times.

(b) In terms of grain refinement, optimization of the sintering process, for example, by two-step sintering or cold sintering is the other approach. In the sintering process, factors such as the rate of heating and the length of the sintering time greatly affect the size of grains and the elimination of pores, thus affecting the breakdown strength and other aspects of energy-storage performance. There are no direct reports of the application of this approach to Bi-based ceramics, therefore, some non-Bi-based examples are listed below. By introducing ST into NN with the help of the two-step sintering method, Xie *et al* [170] decreased the average grain size of 0.83NN-0.17ST ceramics with a relaxed FE rhombohedral phase from 8.2 to 1.2 μm. The recoverable energy-storage density ( $W_{rec}$ ) was greatly increased, by 176%. This approach significantly optimizes the stability of the energy storage of NN-based ceramics. As shown in figure 12, two-step sintering [171] inhibits the grain growth driven by interface energy, causing more grain boundary numbers to be diffused at the grain boundary, densifying the sample and thereby enhancing the insulation. In addition, spark plasma sintering, peak sintering [172], and cold sintering [173] are usually adopted to decrease the sintering temperature and reduce the grain size. It has been reported that cold sintering can inhibit the volatilization of elements, improving various electrical properties.

The domain is another factor that is usually considered to influence the energy storage. Hence, grain orientation has been controlled by the textured template method. By controlling the grain orientation, the strain and stress of ceramic capacitors under strong fields can be reduced, and the breakdown strength caused by microcracks and tensile stress can be avoided, which improves the breakdown strength and energy-storage density. Li *et al* [174] synthesized a <111>-oriented strontium titanate

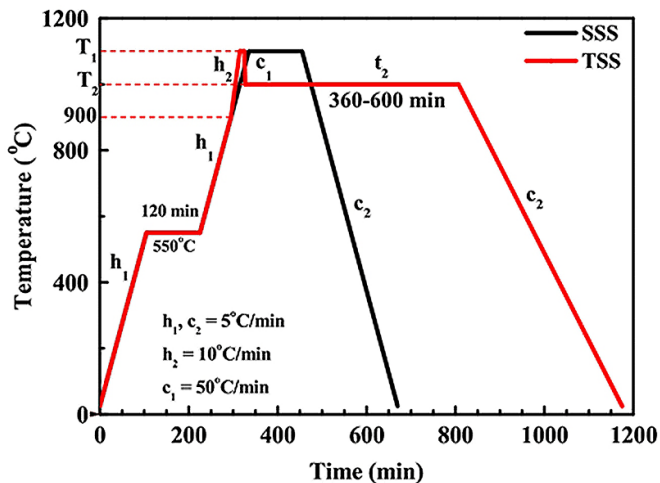


**Figure 12.** The improved sintering process of two-step sintering. Reprinted from [171], Copyright (2015), with permission from Elsevier.

template for the first time. They then successfully fabricated multilayer textured ceramic capacitors with a 91% texture. The electrostriction of the ceramics under a strong field was greatly reduced, a breakdown strength of  $1000 \text{ kV cm}^{-1}$  was obtained, and the energy-storage density was increased to  $21.5 \text{ J cm}^{-3}$ .

In the above, some performance improvement methods for Bi-based energy-storage ceramics have been proposed. In addition, it is worth summarizing some of the usual methods used for non-Bi lead-free energy-storage materials.

#### 4.3. Defect engineering

Another important improvement method is defect engineering, for example, by low-temperature polarization, ion bombardment, etc. Defect dipoles usually affect the energy storage performance. In the volatilization of Bi, the defect dipoles induced by point defects remain after volatilization. The combination of electrons or various ions can cause new phenomena, such as giant dielectric permittivity, high polarization, etc. Defect engineering methods, such as defect doping, have attracted more and more attention for improving the dielectric properties of materials and achieving breakthroughs in other properties. These properties include FE properties, piezoelectric properties, domain engineering controlled by defects, and giant dielectric behavior enhanced by defects. When doping BT with Fe, Liu *et al* [175] proposed an empirical and computationally tractable model, and assumed that the lattice sites occupied by an Fe ion and its six nearest neighbors would lose their ability to polarize, and so this would give rise to a small cluster of defect dipoles. The driving forces behind doping effects suggest that active dipoles which exist in proximity to the defect dipoles can account for experimentally observed phenomena. Dong *et al* [176] also used  $\text{Mg}^{2+}$  ions with a large ion radius to replace  $\text{Ti}^{4+}$  in anatase titanium dioxide, and

found that the electrochemical behavior changed from linear to nonlinear after doping with titanium dioxide, as shown in figure 13. This material showed an abnormal hysteresis in its polarization behavior.

They believed that a local symmetry region was formed by doping the defect dipole. The interaction between the polarizations of these local broken-symmetry regions resulted in a glassy state with an electric dipole, which could lead to nonlinear polarization behavior at room temperature. After polarizing the sample with an electric field, it was found that a dielectric relaxation peak appeared in the corresponding dielectric spectrum versus temperature. The increase in the defect dipoles greatly improved the polarization rate and increased the dielectric permittivity of titanium dioxide. By doping additional defect dipoles, the polarization and the energy-storage properties could be improved.

Moreover, by regulating the defect dipoles, the breakdown strength can be improved. It was reported that the common methods and strategies for improving the breakdown strength of FE materials were as follows [177]: (a) reduce the thickness and electrode area; (b) increase the relative density of the material; (c) increase the bandgap of the material; (d) improve the insulation; (e) implant a dead layer; (f) anneal in oxygen. Although these methods and strategies were very effective for systems containing no volatile elements, such as barium titanate and barium strontium titanate, they were often ineffective for systems containing volatile elements such as BF, KNN, BNT, etc. In terms of nano energy, Peng *et al* [177] recently proposed a general method to improve the breakdown strength of dielectric materials, which was called low-temperature polarization. The material was polarized at the temperature of liquid nitrogen, which allowed the defect dipoles and nanodomains to form a highly ordered structure. Using this method, Peng *et al* found that the breakdown strength of  $(\text{Pb},\text{La})(\text{Zr},\text{Sn},\text{Ti})\text{O}_3$  thin film increased from  $1286$  to  $2000 \text{ kV cm}^{-1}$ , and the corresponding energy-storage density of the thin film also increased from  $16.6$  to  $31.2 \text{ J cm}^{-3}$ , as shown in figure 14.

In addition, increasing the density of defect dipole by ion bombardment, the enhanced energy storage performance has been proposed. Usually, the increasing of defects could have two beneficial effects: reducing leakage and horizontal moving hysteresis loops. By striking the target ion of its lattice site and by purposefully increasing the concentration of intrinsic point defects (such as lead, titanium, oxygen vacancies, etc.), Martin *et al* [178] bombarded the  $0.68\text{Pb}(\text{Mg}_{1/3}\text{Nb}_{2/3})\text{O}_3$ - $0.32\text{PbTiO}_3$  (PMN-PT) membrane with high-energy helium ions, as shown in figure 15. They found that the point defects had reduced the leakage, delayed the low field polarization saturation, promoted the formation of defect dipoles and increased the more complex defect complexes. Meanwhile, it improved the polarization at large field, and enhanced the breakdown strength. The energy storage density of PMN-PT membrane increased to  $133 \text{ J/cm}^3$ , and the efficiency reached to 75%.



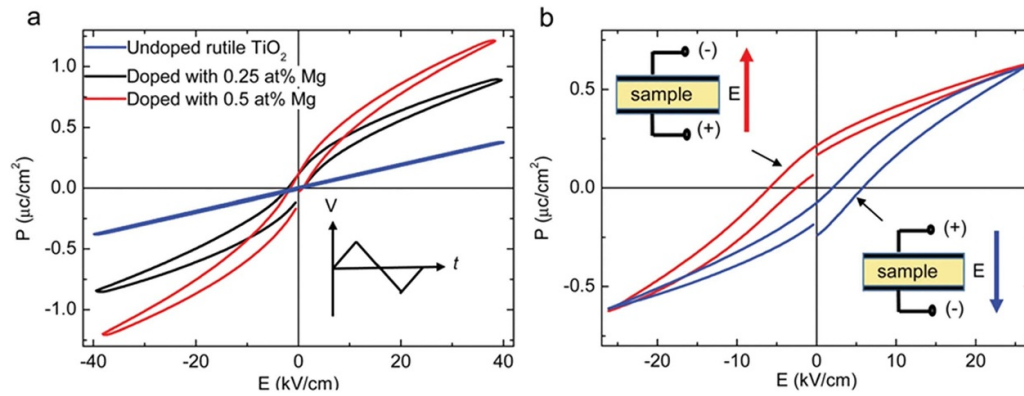


**Figure 13.** Electrochemical behavior change from linear to nonlinear following the doping of  $\text{TiO}_2$ , showing abnormal hysteresis of the polarization behavior. Reproduced from [176] with permission of The Royal Society of Chemistry.

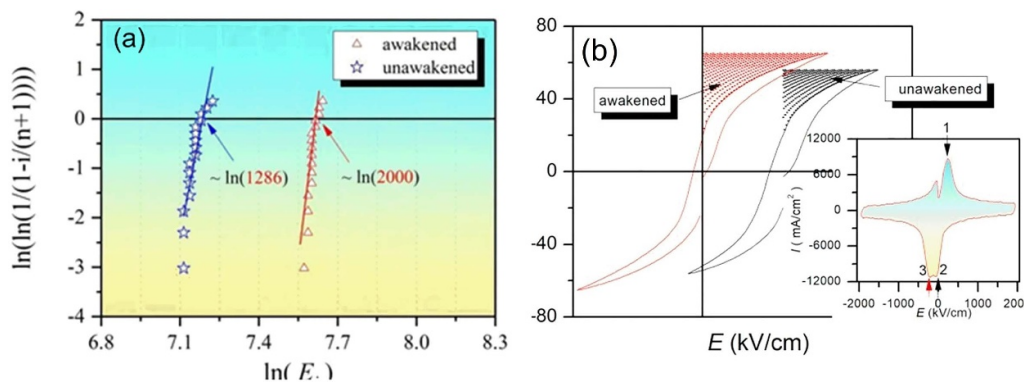


**Figure 14.** Comparison of (a) dielectric breakdown strength (b) energy storage density before polarization (wake-up) and after polarization (wake-up). Reprinted from [177], Copyright (2020), with permission from Elsevier.

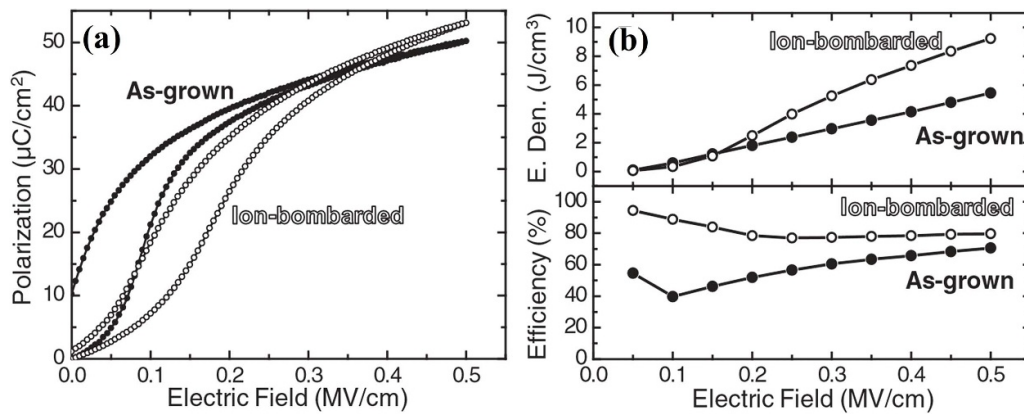


**Figure 15.** Delayed saturation polarization and energy storage characteristics of ion Bombardment [178].

### 5. Summary and perspectives

In the field of dielectric energy storage, lead-free electronic ceramics have become an inevitable trend. Due to the similarity in the properties of  $\text{Bi}^{3+}$  and  $\text{Pb}^{2+}$ , the lone pair of electrons in the outermost  $6s^2$  layer can be hybridized with the  $6p$  vacant orbital or the  $\text{O}^{2-}$  orbital to produce high electron polarizability. In addition, as frequently reported recently, compared to NN-based materials, AN-based AFEs which possess large energy-storage capacity, Bi-based RFE ceramics such as

BNT, BF, etc, have unique advantages, such as their possible use in high-temperature energy storage. Moreover, due to their high polarization (for example,  $100 \mu\text{C cm}^{-2}$ ) which could lead to a large  $P_{\text{max}}$ , the potential energy-storage density of Bi-based materials is higher. In spite of this, based on previous research, the properties of Bi-based ceramics are a long way from meeting the requirements. Methods for improving the energy-storage performance still need more attention. We briefly summarize some of the methods below, in figure 16. In order to increase the energy storage of Bi-based ceramics,

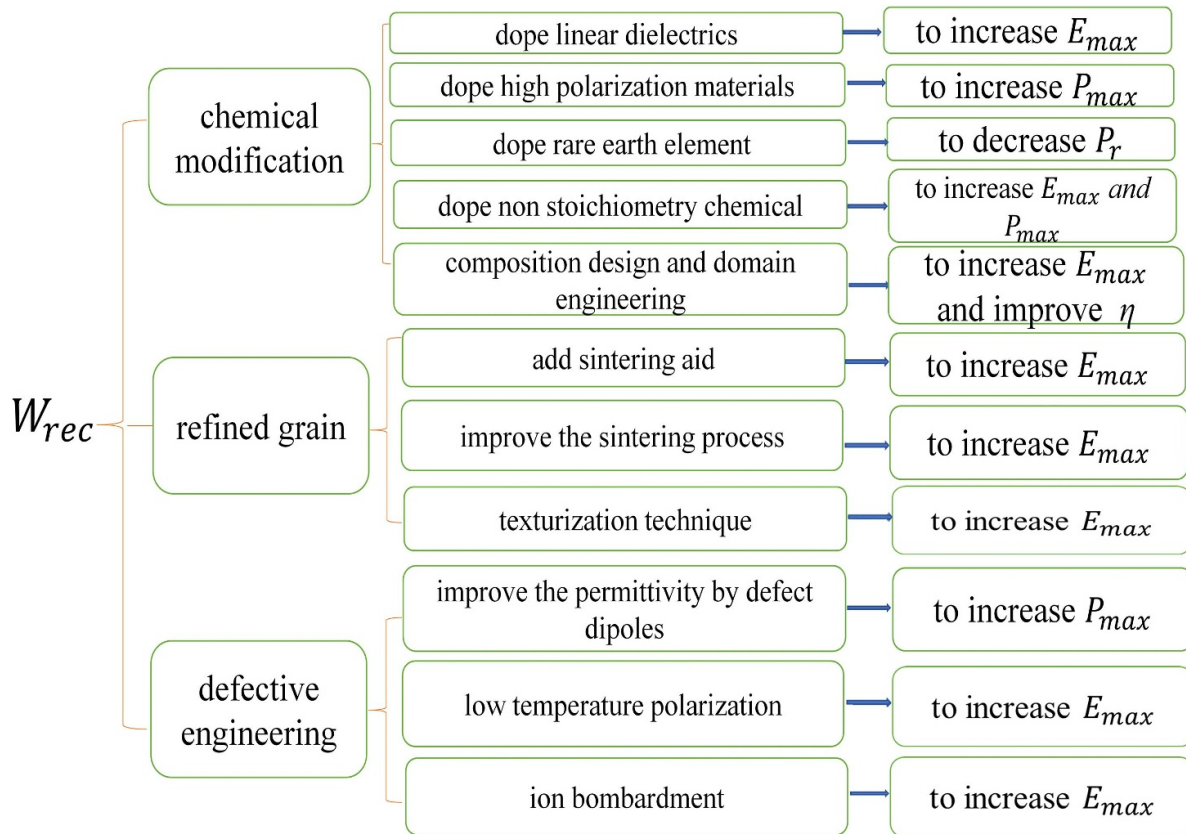


Figure 16. Methods for improving Bi-based energy storage ceramics.

large  $E_{max}$ ,  $\eta$ ,  $P_{max}$ , and small  $P_r$  are required, for which, in summary, chemical modification, grain refinement, and defect engineering are the main methods. We hope that this paper will provide a reference for the field of lead-free energy-storage ceramics.

### Data availability statement

No new data were created or analysed in this study.

### Acknowledgments

The authors gratefully acknowledge the support of the National Natural Science Foundation of China (Nos. 51672092, U1732117 and 51902111), the China Postdoctoral Science Foundation (No. 2019M662602), the Natural Science Foundation of Guangxi (AA138162, GA245006, FA198015, and AA294014), the High-Level Innovation Team and Outstanding Scholar Program of Guangxi Institutes, and the Open Fund of the Guangxi Key Laboratory of Information Materials (No.191015-K). The authors thank the projects supported by the Guangdong HUST Industrial Technology Research Institute, the Guangdong Provincial Key Laboratory of Digital Manufacturing Equipment (2020B1212060014) and the DongGuan Innovative Research Team Program (2020607101007). The authors wish to thank the Analytical and Testing Center of Huazhong University of Science

and Technology for their help with related tests. In particular, the authors appreciate the valuable suggestions and comments made by the the anonymous reviewers and the editor, Professor Huiyun Liu.

### ORCID iDs

Naohisa Takesue <https://orcid.org/0000-0002-5910-6622>  
 Bo Nan <https://orcid.org/0000-0002-6580-7273>  
 Laijun Liu <https://orcid.org/0000-0002-6889-2506>  
 Haibo Zhang <https://orcid.org/0000-0002-5544-531X>

### References

- [1] Winter M and Brodd R J 2004 *Chem. Rev.* **104** 24
- [2] Xie B, Zhang H B, Zhang L, Zhu Y, Guo X, Fan P and Zhang H 2018 *Nano Energy* **54** 437–46
- [3] Arico A S, Bruce P, Scrosati B, Tarascon J-M and Van Schalkwijk W 2005 *Nat. Mater.* **4** 11
- [4] Hao X H 2013 *J. Adv. Dielectr.* **3** 1330001
- [5] Chana K-Y, Jia B H, Lin H, Hameed N, Lee J-H and Lau K-T 2018 *Compos. Struct.* **188** 126–42
- [6] Kumar R A, Priyalakshmi D K and Saroj R 2017 *J. Energy Storage* **13** 10–23
- [7] Wang Y X, Chou S L, Liu H K and Dou S-X 2013 *J. Power Sources* **244** 240–5
- [8] Wei X, Yan H X, Wang T, Hu Q, Viola G, Grasso S, Jiang Q, Jin L, Xu Z and Reece M J 2013 *J. Appl. Phys.* **113** 024103

- [9] Fan P Y, Zhang H B, Liu G, Zang J, Samart C, Zhang T, Tan H, Salamon D, Zhang H and Liu G 2020 *J. Mater. Chem. C* **8** 5681–91
- [10] Luo X, Wang J, Dooner M and Clarke J 2015 *Appl. Energy* **137** 511–36
- [11] Ren G Z, Ma G Q and Cong N 2015 *Renew. Sustain. Energy Rev.* **41** 225–36
- [12] Yao Z H, Song Z, Liu H X, Yu Z, Cao M, Zhang S, Lanagan M T and Liu H 2017 *Adv. Mater.* **29** 1601727
- [13] Yuan J K, Dang Z M, Yao S H, Zha J-W, Zhou T, Li S-T and Bai J 2010 *J. Mater. Chem.* **20** 2441–7
- [14] Tian Y, Hu Q Y, Abrahams I, Yu K, Zhuang Y, Viola G, Abrahams I, Xu Z, Wei X and Yan H 2019 *J. Mater. Chem. A* **7** 834–42
- [15] Wang J H, Li Y, Sun N N, Du J, Zhang Q and Hao X 2019 *J. Eur. Ceram. Soc.* **39** 255–63
- [16] Liang Z S, Ma C R, Shen L K, Lu L, Lu X, Lou X, Liu M and Jia C-L 2019 *Nano Energy* **57** 519–27
- [17] Yang H B, Yan F, Lin Y and Wang T 2018 *J. Eur. Ceram. Soc.* **38** 1367–73
- [18] Yang H B, Yan F, Zhang G, Lin Y and Wang F 2017 *J. Alloys Compd.* **720** 116–25
- [19] Zhang H B, Wei T, Zhang Q, Ma W, Fan P, Salamon D, Zhang S-T, Nan B, Tan H and Ye Z-G 2020 *J. Mater. Chem. C* **8** 16648
- [20] Chen S C *et al* 2013 *J. Mater. Sci., Mater. Electron.* **24** 4764–8
- [21] Li S, Dong X L, Wang G S, Fu Z, Xu C, Xu F, Wang G and Dong X 2021 *Energy Storage Mater.* **34** 417–26
- [22] Jin Q, Pu Y P, Wang C, Gao Z-Y and Zheng H-Y 2017 *Ceram. Int.* **43** S232–8
- [23] Wang H Y, Cao M H, Liu M, Hao H, Yao Z and Liu H 2020 *J. Alloys Compd.* **826** 153891
- [24] Diao C L, Liu H X, Hao H, Cao M and Yao Z 2016 *Ceram. Int.* **42** 12639–43
- [25] Wang T, Jin L, Shu L, Hu Q and Wei X 2014 *J. Alloys Compd.* **617** 399–403
- [26] Wang Y R, Pu Y P, Cui Y, Shi Y and Zheng H 2017 *Mater. Lett.* **201** 203–6
- [27] Liu B B, Wang X H, Zhang R and Li L 2017 *J. Alloys Compd.* **691** 619–23
- [28] Wu T, Pu Y P, Zong T and Gao P 2014 *J. Alloys Compd.* **584** 461–5
- [29] Wang Y, Shen Z Y, Li Y M, Wang Z-M, Luo W-Q and Hong Y 2015 *Ceram. Int.* **41** 8252–6
- [30] Zhao F X, He Q, Bai Q Z, Wu W-J, Wu B and Chen M 2020 *Ceram. Int.* **46** 3257–63
- [31] Huang Y H, Wu Y J, Qiu W J, Li J and Chen X M 2015 *J. Eur. Ceram. Soc.* **35** 1469–76
- [32] Cui C W, Pu Y P, Li X, Cui Y and Liu G 2018 *Mater. Res. Bull.* **105** 114–20
- [33] Zhao P, Tang B, Fang Z, Si F, Yang C and Zhang S 2020 *Chem. Eng. J.* **403** 126290
- [34] Huang Y H, Liu B, Li J and Wu Y J 2019 *Mater. Res. Bull.* **113** 141–5
- [35] Wang T, Jin L, Li C, Hu Q and Wei X 2015 *J. Am. Ceram. Soc.* **98** 559–66
- [36] Zhao X B, Zhou Z Y, Liang R H, Liu F and Dong X 2017 *Ceram. Int.* **43** 9060–6
- [37] Li W B, Zhou D, Li F, Li F, Pang L-X and Lu S-G 2016 *J. Alloys Compd.* **685** 418–22
- [38] Zhang G Z, Zhu D Y, Zhang X S, Zhang L, Yi J, Xie B, Zeng Y, Li Q, Wang Q and Jiang S 2015 *J. Am. Ceram. Soc.* **98** 1175–81
- [39] Chen S, Wang X, Yang T and Wang J 2014 *J. Electroceram.* **32** 307–10
- [40] Zhao Y Y, Yang L, Zhou C R, Zhou C, Lu X, Yuan C, Li Q, Chen G and Wang H 2016 *J. Alloys Compd.* **666** 209–16
- [41] Liu Z C, Ren P R and Long C B 2017 *J. Alloys Compd.* **721** 538–44
- [42] Chen P and Chu B 2016 *J. Eur. Ceram. Soc.* **36** 81–88
- [43] Yang Z T *et al* 2019 *Nano Energy* **58** 768–77
- [44] Wang J, Yang T, Chen S and Li G 2013 *Mater. Res. Bull.* **48** 3847–9
- [45] Chen S *et al* 2013 *J. Mater. Sci., Mater. Electron.* **24** 4764–8
- [46] Yang X, Liu Y, He C, Tailor H and Long X 2015 *J. Eur. Ceram. Soc.* **35** 4173–80
- [47] Zhang L, Jiang S L, Fan B Y and Zhang G 2015 *Ceram. Int.* **41** 1139–44
- [48] Tang M Y *et al* 2020 *Chem. Eng. J.* **29** 12755
- [49] Ren P R, Dong R, Sun L, Yan F, Yang S and Zhao G 2020 *J. Eur. Ceram. Soc.* **40** 4495–502
- [50] Dong X Y *et al* 2020 *J. Materiomics* **3** 629–39
- [51] Liu X D, Hou Y D, Xu Y, Zheng M and Zhu M 2020 *J. Alloys Compd.* **844** 156163
- [52] Sun H N, Lou X J, Sun Q, Zhang X, Ma Z, Guo M, Sun B, Zhu X, Liu Q and Lou X 2020 *J. Eur. Ceram. Soc.* **40** 2929–35
- [53] Song A Z, Wang J, Lv Y, Liang L, Wang J and Zhao L 2019 *Mater. Lett.* **237** 278–81
- [54] Lu Z L *et al* 2021 *Nano Energy* **79** 105423
- [55] Chen H Y, Chen X L, Shi J, Sun C, Dong X, Pang F and Zhou H 2020 *Ceram. Int.* **46** 28407–13
- [56] Wei T *et al* 2021 *Ceram. Int.* **47** 3713–9
- [57] Choi Y, Park J H, Park J-H and Park J-G 2004 *Mater. Lett.* **58** 3102–6
- [58] Shende R V, Krueger D S, Lombardo S J and Lombardo S J 2001 *J. Am. Ceram. Soc.* **84** 1648–50
- [59] Smolensky G A *et al* 1961 *Sov. Phys. Solid State* **2** 2651–4
- [60] Li D X *et al* 2020 *J. Mater. Sci., Mater. Electron.* **31** 3648–53
- [61] Wu J G 2020 *J. Appl. Phys.* **127** 190901
- [62] Zhang S T, Kounga A B, Aulbach E, Granzow T, Jo W, Kleebe H-J and Rödel J 2008 *J. Appl. Phys.* **103** 034107
- [63] Yuan Q B *et al* 2018 *Nano Energy* **52** 203–10
- [64] Bührer C F 1962 *J. Chem. Phys.* **36** 798–803
- [65] Barick B K and Pradhan D K 2013 *Ceram. Int.* **39** 5695–704
- [66] Damjanovic D, Klein N, Li J and Porokhonskyy V 2010 *Funct. Mater. Lett.* **3** 5–13
- [67] Li D X *et al* 2019 *J. Mater. Sci., Mater. Electron.* **30** 5917–22
- [68] Zvirgzds J A, Kapostin P P, Zvirgzde J V and Kruzina T V 1982 *Ferroelectrics* **40** 75–77
- [69] Zhang M S, Scott J F and Zvirgzds J A 2005 *Ferroelectrics* **315** 123–47
- [70] Lu W Z, Wang Y, Liang F, Wang X and Liang F 2011 *J. Alloys Compd.* **509** 2738–44
- [71] Brianti S, Chen C N, Chou C C, Liang J-Y, Chen P-Y and Chen C-S 2013 *Ceram. Int.* **39** S175–9
- [72] Sakata K and Masuda Y 1974 *Ferroelectrics* **7** 347–9
- [73] Jones G O and Thomas P A 2002 *Acta Cryst. B* **58** 168–78
- [74] Suchanicz J and Kwapulinski J 1995 *Ferroelectrics* **65** 249–53
- [75] Wu J Y, Zhang Z, Huang C-H, Tseng C-W, Meng N, Koval V, Chou Y-C, Zhang Z and Yan H 2020 *Nano Energy* **76** 105037
- [76] Vakhrushev S B, Isupov V A, Kvyatkovsky B E, Okuneva N M, Pronin I P, Smolensky G A and Szymonov P P 1985 *Ferroelectrics* **63** 153–60
- [77] Ma C and Tan X 2010 *Solid State Commun.* **150** 1497–500
- [78] Isupov V A 2005 *Ferroelectrics* **15** 123–47
- [79] Kling J, Tan X, Jo W, Kleebe H-J, Fuess H and Rödel J 2010 *J. Am. Ceram. Soc.* **93** 2452–5
- [80] Hinterstein M, Knapp M, Hölzel M, Jo W, Cervellino A, Ehrenberg H and Fuess H 2010 *J. Appl. Crystallogr.* **43** 1314–21
- [81] Jo W, Granzow T, Aulbach E, Rödel J and Damjanovic D 2009 *J. Appl. Phys.* **105** 094102
- [82] Schmitt L A and Kleebe H J 2010 *Funct. Mater. Lett.* **3** 55–58



- [83] Dorcet V, Trolliard G and Boullay P 2008 *Chem. Mater.* **20** 5061–73
- [84] Liu L, Knapp M, Ehrenberg H, Fang L, Schmitt L A, Fuess H, Hoelzel M and Hinterstein M 2016 *J. Appl. Crystallogr.* **49** 574–84
- [85] Liu L *et al* 2017 *J. Eur. Ceram. Soc.* **37** 1387–99
- [86] Tai C W, Hong C S and Chan H L 2010 *J. Am. Ceram. Soc.* **91** 3335–41
- [87] Jo W, Schaab S, Sapper E, Schmitt L A, Kleebe H-J, Bell A J and Rödel J 2011 *J. Appl. Phys.* **110** 1153–62
- [88] Viola G, Ning H, Wei X, Deluca M, Adomkevicius A, Khaliq J, John Reece M and Yan H 2013 *J. Appl. Phys.* **114** 168–76
- [89] Dorcet V, Trolliard G and Boullay P 2009 *J. Magn. Magn. Mater.* **321** 1758–61
- [90] Ma C, Tan X, Dul'kin E and Roth M 2010 *J. Appl. Phys.* **108** 104105
- [91] Qi H and Zuo R Z 2019 *J. Mater. Chem. A* **7** 3971–8
- [92] Gao F, Dong X, Mao C, Liu W, Zhang H, Yang L, Cao F and Wang G 2011 *J. Am. Ceram. Soc.* **94** 4382–6
- [93] Gao F, Dong X, Mao C, Cao F and Wang G 2011 *J. Am. Ceram. Soc.* **94** 4162–4
- [94] Viola G, Ning H, Reece M J, Wilson R, Correia T M, Weaver P, Cain M G and Yan H 2012 *J. Phys. D: Appl. Phys.* **45** 355302
- [95] Zhang L, Hao X and Zhang L 2014 *Ceram. Int.* **40** 8847–51
- [96] Yao Y, Li Y, Sun N, Du J, Li X, Zhang L, Zhang Q and Hao X 2018 *J. Alloys Compd.* **750** 228–34
- [97] Chen P, Li P, Zhai J W, Shen B, Li F and Wu S 2017 *Ceram. Int.* **43** 13371–6
- [98] Li M, Fan P Y, Zhang H B, Liu K, Zang J, Samart C, Zhang T, Tan H, Salamon D and Zhang H 2019 *J. Mater. Chem. C* **7** 15292
- [99] Chandrasekhar M and Kumar P 2015 *Ceram. Int.* **41** 5574–80
- [100] Wang Y, Lv Z, Xie H and Cao J 2014 *Ceram. Int.* **40** 4323–6
- [101] Xu Q, Li T, Hao H, Zhang S, Wang Z, Cao M, Yao Z and Liu H 2015 *J. Eur. Ceram. Soc.* **35** 545–53
- [102] Takenaka T and Nagata H 2005 *J. Eur. Ceram. Soc.* **25** 2693–700
- [103] Li D X, Shen Z Y, Li Z, Luo W, Song F, Wang X, Wang Z and Li Y 2020 *J. Mater. Chem. C* **8** 7650–7
- [104] Ma W G, Fan P Y, Zhang H B, Kongparakul S, Samart C, Zhang T, Zhang G, Jiang S, Chang J-J and Zhang H 2019 *Ceram. Int.* **45** 19895–901
- [105] Cao W P, Li W, Fei L, Zhang T D, Sheng J, Hou Y F and Fei W D 2016 *J. Eur. Ceram. Soc.* **36** 593–600
- [106] Li Q N *et al* 2016 *J. Mater. Sci., Mater. Electron.* **27** 10810–5
- [107] Chen M, Xu Q, Kim B H, Ahn B K, Ko J H, Kang W J and Nam O J 2008 *J. Eur. Ceram. Soc.* **28** 843–9
- [108] Liu L, Fang L, Schmitt L A, Ehrenberg H, Fang L, Fuess H, Hoelzel M and Hinterstein M 2016 *Europhys. Lett.* **114** 47011
- [109] Liu L, Ma X, Knapp M, Ehrenberg H, Peng B, Fang L and Hinterstein M 2017 *Europhys. Lett.* **118** 47001
- [110] Borkar H, Singh V N, Singh B P, Tomar M, Gupta V and Kumar A 2014 *RSC Adv.* **4** 22840–7
- [111] Xu Y, Liu X, Wang G, Liu X and Feng Y 2016 *Ceram. Int.* **42** 4313–22
- [112] Wu J Y, Zhang Z, Yan H X, Zhang H, Yang B, Meng N, Zhang Z and Yan H 2018 *Nano Energy* **50** 723–32
- [113] Lin D *et al* 2006 *Appl. Phys. Chem. C* **88** 062901
- [114] Mishra A, Majumdar B and Ranjan R 2017 *J. Eur. Ceram. Soc.* **37** 2379–84
- [115] Ma W G, Zhang H B, Marwat M A, Fan P, Xie B, Salamon D, Ye Z-G and Zhang H 2018 *J. Mater. Chem. C* **7** 281–8
- [116] Smolensky G A *et al* 1959 *Sov. Phys. Solid State* **1** 149–50
- [117] Teague J R, Gerson R and James W J 1970 *Solid State Commun.* **8** 1073–4
- [118] Smolenskii G A *et al* 1958 *Sov. Phys. Solid State* **3** 1981–3
- [119] Kaczmarek W, Pajk Z and Polomski A M 1975 *Solid State Commun.* **17** 807–10
- [120] Kumar M M, Palkar V R, Srinivas K and Suryanarayana S V 2000 *Appl. Phys. Lett.* **76** 2764–6
- [121] Neaton J B, Ederer C, Waghmare U V, Spaldin N A and Rabe K M 2005 *Phys. Rev. B* **71** 014113
- [122] Zavaliche F, Yang S Y, Zhao T, Chu Y H, Cruz M P, Eom C B and Ramesh R 2006 *Phase Transit.* **79** 991–1017
- [123] Wang J, Neaton J and Zheng H 2003 *Science* **299** 1719–22
- [124] Lebeugle D, Colson D, Forget A, Viret M, Bonville P, Marucco J F and Fusil S 2007 *Phys. Rev. B* **76** 024116
- [125] Yun K Y, Okuyama M, Okuyama M, Saeki H, Tabata H and Saito K 2004 *J. Appl. Phys.* **96** 3399–403
- [126] Hang J X *et al* 2011 *Phys. Rev. Lett.* **107** 147602
- [127] Zheng D G and Zuo R Z 2016 *J. Eur. Ceram. Soc.* **1** 413–8
- [128] Xu B, Bellaiche L and Bellaiche L 2017 *Nat. Commun.* **8** 15682
- [129] Callisir I, Kleppe A K, Kleppe A K and Hall D A 2018 *J. Mater. Chem. A* **6** 5378–9
- [130] Pan H *et al* 2018 *Nat. Commun.* **9** 1813
- [131] Lee M H, Kim D J, Park J S, Kim S W, Song T K, Kim M-H, Kim W-J, Do D and Jeong I-K 2015 *Adv. Mater.* **27** 6976–82
- [132] Zhu L F *et al* 2017 *J. Alloys Compd.* **16** 20266–75
- [133] Correia T M, Viola G, Rokosz M K, Weaver P M, Gregg J M, Viola G and Cain M G 2013 *J. Am. Ceram. Soc.* **96** 2699–702
- [134] Zhu L F, Lei X W, Zhao L, Hussain M I, Zhao G-Z and Zhang B-P 2019 *Ceram. Int.* **45** 20266–75
- [135] Kumar M M, Srinivas A and Suryanarayana S V 2000 *J. Appl. Phys.* **87** 855–62
- [136] Liu N, Dong X L, Zhou Z and Dong X 2018 *J. Mater. Chem. C* **6** 10211–7
- [137] Zhang D, Zuo R Z, Zhang D and Li Y 2015 *J. Am. Ceram. Soc.* **98** 2692–295
- [138] Liu N, Liang R, Zhao X, Xu C, Zhou Z and Dong X 2018 *J. Am. Ceram. Soc.* **101** 3259–65
- [139] Wang D W, Fan Z, Zhou D, Khesro A, Murakami S, Feteira A, Zhao Q, Tan X and Reaney I 2018 *J. Mater. Chem. A* **6** 4133–44
- [140] Fujino S, Murakami M, Anbusathaiah V, Lim S-H, Nagarajan V, Fennie C J, Wuttig M, Salamanca-Riba L and Takeuchi I 2008 *Appl. Phys. Lett.* **92** 202904
- [141] Yang H G, Qi H and Zuo R Z 2019 *J. Eur. Ceram. Soc.* **39** 2673–9
- [142] Wang G *et al* 2019 *Energy Environ. Sci.* **12** 582
- [143] Chen Z T *et al* 2020 *Ceram. Int.* **46** 11549–55
- [144] Zhou M X, Liang R H, Zhou Z and Dong X 2018 *J. Mater. Chem. C* **6** 8528–37
- [145] Zhou H F, Chen X, Sun C, Pang F, Chen H, Dong X, Zhou X, Wang K and Zhou H 2020 *Ceram. Int.* **46** 25731–7
- [146] Zhou X F, Qi H, Zhang D, Xue G, Luo H and Zhang D 2019 *J. Eur. Ceram. Soc.* **39** 4053–9
- [147] Hu Q Y, Li J, Wei X Y, Li C, Xing Z and Wei X 2015 *J. Alloys Compd.* **640** 416–20
- [148] Li J, Li F, Xu Z and Zhang S 2018 *Adv. Mater.* **30** 1802155
- [149] Zhao P *et al* 2020 *J. Mater.* **7** 195–207
- [150] Zhang G, Cao M, Hao H and Liu H 2013 *Ferroelectrics* **447** 821910
- [151] Chao M M, Liu J S, Zhang S R, Wang D, Yu H, Yuan Y and Zhang S 2018 *Appl. Phys. Lett.* **112** 203903
- [152] Zhao P, Tang B, Zhang S R, Yang C, Li H and Zhang S 2020 *J. Eur. Ceram. Soc.* **40** 1938–46
- [153] Ding J 2020 *Ceram. Int.* **46** 14816–21
- [154] Kong X *et al* 2020 *Materials* **13** 18
- [155] Chen P *et al* 2019 *J. Eur. Ceram. Soc.* **36** 81–8
- [156] Li F, Zhai J W, Zeng W R, Liu X, Yang K, Zhang, Y, Li P, Liu B and Zeng H 2017 *J. Appl. Phys.* **121** 054103



- [157] Zhang J T, Li Y, Yuan Q B, Yang Y, Yang H and Yuan Q 2020 *J. Eur. Ceram. Soc.* **40** 5458–65
- [158] Li D X, Shen Z Y, Li Z, Luo W, Wang X, Wang Z, Song F and Li Y 2019 *J. Adv. Ceram.* **9** 183–92
- [159] Uchino K and Nomura S 1982 *Ferroelectrics* **44** 55–61
- [160] Wang T, Jin L, Tian Y, Shu L, Hu Q and Wei X 2014 *Mater. Lett.* **137** 79–81
- [161] Xu Z X, Hao X H and An S L 2015 *J. Alloys Compd.* **639** 387–92
- [162] Shiga M, Hagiwara M and Fujihara S 2020 *Ceram. Int.* **46** 10242–9
- [163] Zhang Y L, Li W, Qiao Y, Zhao Y, Wang Z, Yu Y, Xia H, Li Z and Fei W 2018 *Appl. Phys. Lett.* **112** 093902
- [164] Cui C W, Pu Y P, Cui Y F, Wan J, Guo Y, Hui C, Wang Y and Cui Y 2017 *J. Alloys Compd.* **711** 319–26
- [165] Yan F, Jiang T, Zhai J W, Zhou X, Shi Y, Ge G, Shen B and Zhai J 2020 *Energy Storage Mater.* **30** 392–400
- [166] Qi H, Xie A, Zuo R Z and Zuo R 2019 *Adv. Energy Mater.* **10** 1903338
- [167] Liu M, Cao M H, Yao Z H, Qi J, Liu H, Hao H and Yao Z 2018 *Ceram. Int.* **44** 20239–44
- [168] Shen Z Y, Wang Y, Tang Y, Yu Y, Luo W-Q, Wang X, Li Y, Wang Z and Song F 2019 *J. Materiomics* **5** 641–8
- [169] Xiao S, Xiu S, Zhang W, Shen B, Zhai J and Zhang Y 2016 *J. Alloys Compd.* **675** 15–21
- [170] Xie A *et al* 2020 *ACS Appl. Mater. Interfaces* **12** 19267–475
- [171] Bafandeha M R, Wahyudi O, Li Y and Gu H 2015 *Ceram. Int.* **41** 162–70
- [172] Zhang S J *et al* 2020 *ACS Appl. Mater. Interfaces* **12** 32834–41
- [173] Ma J Z, Lin Z, Wu X, Lin C, Wu X, Lin T, Zheng X and Yu X 2019 *J. Eur. Ceram. Soc.* **39** 986–93
- [174] Li J L *et al* 2020 *Nat. Mater.* **19** 999–1005
- [175] Liu J, Wang D, Jiang Z, Liu L, Himanen L, Wei J, Zhang N, Wang D and Jia C-L 2018 *J. Chem. Phys.* **149** 244122
- [176] Dong D *et al* 2019 *Mater. Horiz.* **6** 1717–1725
- [177] Peng B L *et al* 2020 *Nano Energy* **77** 105132
- [178] Kim J, Martin L W, Acharya M, Velarde G, Parsonnet E, Donahue P, Qualls A, Garcia D and Martin L W 2020 *Science* **369** 81–84